Numerical Simulation of Fluid-Structure Interaction Based on Monolithic Variational Formulations

Th. Dunne R. Rannacher Th. Richter

Institute of Applied Mathematics
University of Heidelberg, INF 293/294
D-69120 Heidelberg, Germany

June 15, 2009

Abstract

The dilemma in modeling the coupled dynamics of fluid-structure interaction (FSI) is that the fluid model is normally based on an Eulerian perspective in contrast to the usual Lagrangian formulation of the solid model. This makes the setup of a common variational description difficult. However, such a variational formulation of FSI is needed as the basis of a consistent Galerkin discretization with a posteriori error control and mesh adaptation, as well as the solution of optimal control problems based on the Euler-Lagrange approach. This article surveys recent developments in the numerical approximation of FSI problems based on "monolithic" variational formulations. The modeling is based either on an arbitrary Lagrangian-Eulerian (ALE) or a fully Eulerian-Eulerian (Eulerian) description of the (incompressible) fluid and the (elastic) structure dynamics. These global one-field formulations constitute a strongly implicit coupling of the dynamics of fluid and structure which, in contrast to the commonly used weakly coupled two-field formulations, provides the basis for a robust and efficient solution process. In this context a fully consistent treatment of mesh adaptation (DWR method) and optimal control ("all-at-once" approach) becomes possible within a Galerkin finite element discretization.

1 Introduction

Computational fluid dynamics and computational structure mechanics are two major areas of numerical simulation of physical systems. With the introduction of high performance computing it has become possible to tackle systems with a coupling of fluid and structure dynamics. General examples of such fluid-structure interaction (FSI) problems are flow transporting elastic particles (particulate flow), flow around elastic structures (airplanes, submarines) and flow in elastic structures (haemodynamics, transport of fluids in closed containers). In all these settings the dilemma in modeling the coupled dynamics is that the fluid model is normally based on an Eulerian perspective in contrast to the usual Lagrangian approach for the solid model. This makes the setup of a common variational description difficult. However, such

a variational formulation of FSI is needed as the basis of a consistent approach to residual-based a posteriori error estimation and mesh adaptation as well as to the solution of optimal control problems by the Euler-Lagrange method. This is the subject of the present paper, which is largely based on the doctoral dissertation of the first author Dunne [22] and the survey article Dunne and Rannacher [24].

Combining the Eulerian and the Lagrangian setting for describing FSI involves conceptional difficulties. On the one hand the fluid domain itself is time-dependent and depends on the deformation of the structure domain. On the other hand, for the structure the fluid boundary values (velocity and the normal stress) are needed. In both cases values from the one problem are used for the other, which is costly and can lead to a drastic loss of accuracy. A common approach to dealing with this problem is to separate the two models, solve each separately, and so converge iteratively to a solution which satisfies both together with the interface conditions (Figure 1). Solving the separated problems serially multiple times is referred to as a "partitioned (or segregated) approach".

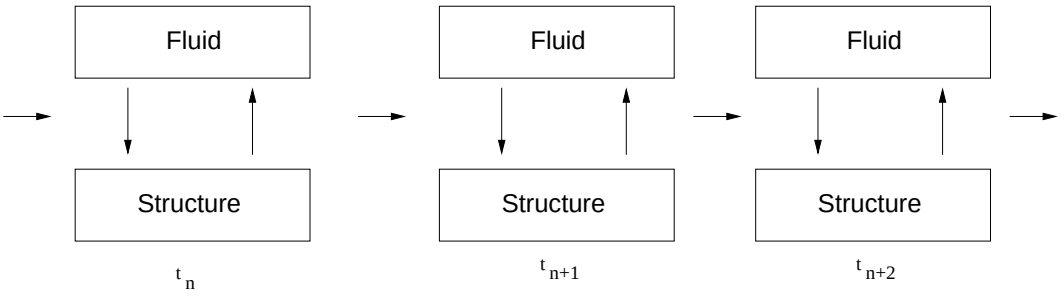

Figure 1: *Partitioned approach, Lagrangian and Eulerian frameworks coupled.*

A partitioned approach does not contain a variational equation for the fluid-structure interface. To achieve this, usually an auxiliary unknown coordinate transformation function T_f is introduced for the fluid domain. With its help the fluid problem is rewritten as one on the transformed domain which is fixed in time. Then, all computations are done on the fixed reference domain and as part of the computation the auxiliary transformation function T_f has to be determined at each time step. Figure 2 illustrates this approach for the driven cavity problem considered in Section 8, below. Such, so-called "arbitrary Lagrangian-Eulerian" (ALE) methods are used in Huerta and Liu [35], Wall [58], Hron, Turek [33], and corresponding transformed space-time finite element formulations in Tezduyar, Behr, Liou [51, 52] and Tezduyar, Sathe, Stein, Aureli [53]. For other ways of dealing with implicit coupling in FSI models, we refer to Vierendeels [56] and Wall, Gerstenberger, Gamnitzer, Forster, Ramm [59]. Computational comparisons of partitioned and monolithic approaches have recently been made in Heil, Hazel, Boyle [30].

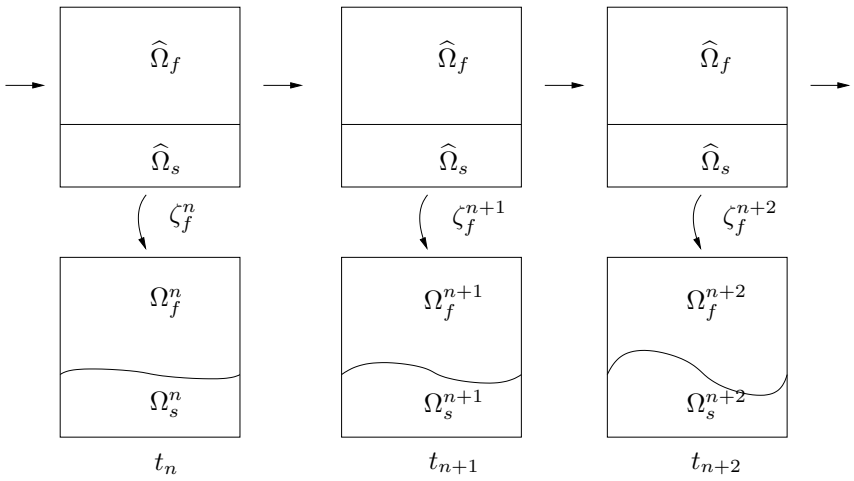

Figure 2: *Transformation approach, both frameworks Lagrangian*

Both, the partitioned and the transformation approach to overcome the Euler-Lagrange discrepancy explicitly track the fluid-structure interface by mesh adjustment and are generally referred to as "interface tracking" methods. Both methods leave the structure problem in its natural Lagrangian setting.

However, one may follow the alternative way of posing the fluid as well as the structure problem in a fully Eulerian-Eulerian (Eulerian) framework. A similar approach has been used by Lui and Walkington [43] in the context of the transport of visco-elastic bodies in a fluid. In the Eulerian setting a phase variable is employed on the fixed mesh to distinguish between the different phases, liquid and solid. This approach to identifying the fluid-structure interface is generally referred to as "interface capturing", a method commonly used in the simulation of multiphase flows, Joseph and Renardy [40]. Examples for the use of such a phase variable are the Volume of Fluid (VoF) method [32] and the Level Set (LS) method Chang, Hou, Merriman, and Osher [16], Osher and Sethian [44], Sethian [49]. In the classical LS approach the distance function has to continually be reinitialized, due to the smearing effect by the convection velocity in the fluid domain. This makes the use of the LS method delicate for modeling FSI problems particularly in the presence of cornered structures. To cope with this difficulty, in Dunne [21, 22] a variant of the LS method, the Initial Position (IP) method, has been proposed that makes reinitialization unnecessary and which easily copes with cornered structures. This approach does not depend on the specific structure model.

The key variable in structure dynamics is the deformation, and since this depends on the deflection, it is understandable why structure dynamics is preferably described in the Lagrangian frame. The set of "initial positions" (IP set) of all structure points enables us to describe the deformations in the Eulerian frame. This set is then transported with the structure velocity in each time step. Based on this concept the displacement is now available in an Eulerian sense. Also its gradient has to be rewritten appropriately, which will be explained in Section 4.2 below. Since the

fluid-structure interface will be crossing through cells, we will have to also transport the IP set in the fluid domain.

If we were to use the fluid velocity for the advection of the IP set, this would lead to entanglement of the respective displacements, which would "wreak havoc" on the interface cells. This is a known problem with LS approaches. A common way for fixing this problem has been to occasionally fix the LS field between the time steps. The problem with this approach is that the variational formulation is no longer consistent. As an alternative, we harmonically continue the structure velocity into the fluid domain. In the fluid domain, we then use this velocity for advecting the IP set. Since an IP set is available in both domains, we can always at each point determine if it belongs to the fluid or solid part of the model.

Again this approach is similar to the LS approach. Actually, it is possible to also develop a model for FSI using the level set approach, Legay, Chessa, and Belytschko [41]. But when developing a complete variational formulation the two key characteristics of the LS approach also become the main cause of concern: reinitialization and the signed distance function. Although the problem of reinitialization here can also be avoided by using an harmonically extended velocity, the trouble concerning corner approximation persists. In contrast to this, by using an initial position set, we are deforming a virtual mesh of the structure which is extended into the whole domain.

The equations we use are based on the momentum and mass conservation equations for the flow of an incompressible Newtonian fluid and the deformation of a compressible St. Venant-Kirchhoff or likewise incompressible neo-Hookean solid. The spatial discretization is by a second-order finite element method with conforming equal-order (bilinear) trial functions using "local projection stabilization", Becker and Braack [4, 5]. The time discretization uses the second-order "Fractional-Step-θ" scheme originally proposed by Bristeau, Glowinski, and Periaux [13]. This method has the same complexity as the Crank–Nicolson scheme but better stability properties, Rannacher [46].

Based on the Eulerian variational formulation of the FSI system, we use the "dual weighted residual" (DWR) method, described in Becker, Rannacher [7, 9, 8], Becker, Heuveline, Rannacher [6], Bangerth, Rannacher [2], Braack, Richter [10], to derive "goal-oriented" a posteriori error estimates. The evaluation of these error estimates requires the approximate solution of a linear dual variational problem. The resulting a posteriori error indicators are then used for automatic local mesh adaptation. The full application of the DWR method to FSI problems requires a Galerkin discretization in space as well as in time. Due to the use of a difference scheme in time, in this paper we are limited to "goal-oriented" mesh adaptation in computing steady states or (somewhat heuristically) to quasi-steady states within the time stepping process. The incorporation of automatic time-step control will be the subject of forthcoming work.

The method for computing FSI described in this paper is validated at a stationary model problem that is a lid-driven cavity involving the interaction of an incompressible Stokes fluid with a linearized incompressible neo-Hookean solid. Then, as a more challenging test the self-induced oscillation of a thin elastic bar immersed in an incompressible fluid is treated (FLUSTRUK-A benchmark, Hron and Turek [34]).

For this test problem, our method is also compared against a standard "arbitrary Lagrange Eulerian" (ALE) approach. The possible potential of the fully Eulerian formulation of the FSI problems is indicated by its good behavior for large structure deformations. All computations and visualizations are done using the flow-solver package GASCOIGNE [26] and the graphics package VISUSIMPLE [57]. The details on the software implementation can be found in Dunne [21, 22, 23].

The outline of this paper is as follows. Section 2 ("Notation") introduces the basic notation for the ALE as well as the Eulerian formulation of the FSI problem and Section 3 ("Reference frameworks") discusses the reference frameworks, *Lagrangian* and *Eulerian*, which will be used throughout this paper. The corresponding variational formulations are developed in detail, first separately for the structure and fluid parts in Section 4 ("Variational formulations of fluid and structure problems") and then for the coupled FSI problem in Section 5 ("Variational formulations of the FSI problem"). Section 6 ("Discretization") describes the discretization in space and time as well as the techniques for solving the algebraic systems and for evaluating directional derivatives. The derivation of a posteriori error estimates and strategies for mesh adaptation is explained in Section 7 ("Mesh adaptation"). In Section 8 ("Numerical test 1: elastic flow cavity") the newly proposed Eulerian method is validated at a stationary test problem "elastic flow cavity". Then, Section 9 ("Numerical test 2: FSI benchmark FLUSTRUK-A") contains the results obtained by the two approaches, ALE and Eulerian, for the solution of the benchmark problem FLUSTRUK-A (oscillations of a thin elastic bar) for various combinations of material models and flow conditions. The paper is closed by Section 10 ("Summary and future development") which gives a summary and points at some directions of ongoing and future research on the basis of the approaches described in this paper.

2 Notation

We begin with introducing some notation which will be used throughout this paper. By $\Omega \subset \mathbb{R}^d$ ($d = 2$ or $d = 3$), we denote the domain of definition of the FSI problem. The domain Ω is supposed to be *time independent* but to consist of two possibly time-dependent subdomains, the fluid domain $\Omega_f(t)$ and the structure domain $\Omega_s(t)$. Unless needed, the explicit time dependency will be skipped in this notation. The boundaries of Ω, Ω_f, and Ω_s are denote by $\partial\Omega$, $\partial\Omega_f$, and $\partial\Omega_s$, respectively. The common interface between Ω_f and Ω_s is $\Gamma_i(t)$, or simply Γ_i.

The initial structure domain is denoted by $\widehat{\Omega}_s$. Spaces, domains, coordinates, values (such as pressure, displacement, velocity) and operators associated to $\widehat{\Omega}_s$ (or $\widehat{\Omega}_f$) will likewise be indicated by a "hat".

Partial derivatives of a function f with respect to the i-th coordinate are denoted by $\partial_i f$, and the total time-derivative by $d_t f$. The divergence of a vector and tensor is written as $\mathrm{div} f = \sum_i \partial_i f_i$ and $(\mathrm{div} F)_i = \sum_j \partial_j F_{ij}$. The gradient of a vector valued function v is the tensor with components $(\nabla v)_{ij} = \partial_j v_i$.

By $[f]$, we denote the jump of a (possibly discontinuous) function f across an interior boundary, where n is always the unit vector n at points on that boundary.

For a set X, we denote by $L^2(X)$ the Lebesque space of square-integrable func-

tions on X equipped with the usual inner product and norm

$$(f,g)_X := \int_X fg\,dx, \quad \|f\|_X^2 = (f,f)_X,$$

respectively, and correspondingly for vector- and matrix-valued functions. Mostly the domain X will be Ω, in which case we will skip the domain index in products and norms. For Ω_f and Ω_s, we similarly indicate the associated spaces, products, and norms by a corresponding index "f" or "s".

We will generally use roman letters, V, for denoting spaces of functions depending only on spatial variables and calligraphic letters, $\mathcal{V}$, for spaces of functions depending additionally on time. Let $L_X := L^2(X)$ and $L_X^0 := L^2(X)/\mathbb{R}$. The functions in L_X (with $X = \Omega$, $X = \Omega_f(t)$, or $X = \Omega_s(t)$) with first-order distributional derivatives in L_X make up the Sobolev space $H^1(X)$. Further, $H_0^1(X) = \{v \in H^1(X) : v_{|\partial X_D} = 0\}$, where ∂X_D is that part of the boundary ∂X at which Dirichlet boundary conditions are imposed. Further, we will use the function spaces $V_X := H^1(X)^d$, $V_X^0 := H_0^1(X)^d$, and for time-dependent functions

$$\begin{aligned} \mathcal{L}_X &:= \mathcal{L}^2[0,T;L_X], \quad \mathcal{V}_X := \mathcal{L}^2[0,T;V_X] \cap \mathcal{H}^1[0,T;V_X^*], \\ \mathcal{L}_X^0 &:= \mathcal{L}^2[0,T;L_X^0], \quad \mathcal{V}_X^0 := \mathcal{L}^2[0,T;V_X^0] \cap \mathcal{H}^1[0,T;V_X^*], \end{aligned}$$

where V_X^* is the dual of V_X^0, and $\mathcal{L}^2$ and $\mathcal{H}^1$ indicate the corresponding properties in time. Again, the X-index will be skipped in the case of $X = \Omega$, and for $X = \Omega_f$ and $X = \Omega_s$ a corresponding index "f" or "s" will be used.

3 Reference frameworks

In modeling the variation of a spatial continuum in time two approaches are commonly used. The *Lagrangian* or *material* framework and the *Eulerian* or *spatial* framework. Both approaches have the simple goal of describing how a certain scalar quantity of interest $f : \mathbb{R}^d \times I \to \mathbb{R}$ changes in space and with time. The choice of the "reference point" of the value f is what distinguishes the two frameworks. We denote by $x \in \mathbb{R}^d$ and $t \in I$ the spatial and temporal coordinates, respectively. The function f is assumed to be sufficiently smooth with respect to space and time.

3.1 Lagrangian framework

In the Lagrangian framework one observes the value at a preselected point that is moving (and possibly accelerating) steadily through space. The initial position of the point at the initial time t_0, we define as $\hat{x}$. Thus, the position of the point is a function of the initial position $\hat{x}$ and time t,

$$x = x(\hat{x}, t).$$

We define the velocity v of this point as the total time derivative of its position x,

$$v(x,t) := d_t x(\hat{x},t) = \partial_t x + \hat{\nabla} x\, d_t \hat{x}. \tag{3.1}$$

Since $\hat{x}$ is the position of the point at an initial time it follows that it does not change in time, i.e., $d_t\hat{x} = 0$ and $v = \partial_t x$.

To be more precise, in the Lagrangian framework we should refer to $f(x,t)$ as $\hat{f}(\hat{x},t) := f(x(\hat{x},t),t)$. Visually one can imagine that we are observing the value at a *material point* that was initially at the position $\hat{x}$ and is moving through space with velocity v. The total time derivative of $\hat{f}$ in the Lagrangian framework can thus be written:

$$d_t\hat{f}(\hat{x},t) = \partial_t\hat{f}(\hat{x},t) + \hat{\nabla}\hat{f}(\hat{x},t)\, d_t\hat{x} = \partial_t\hat{f}(\hat{x},t). \tag{3.2}$$

Since the Lagrangian approach describes the movement and deformation of individual particles and volumes it follows that this framework is the natural approach for modeling structure dynamics.

3.2 Eulerian framework

In the Eulerian framework one observes the value at a fixed point x in space. Hence this framework is also referred to as a *spatial framework*. Looking back at the Lagrangian framework one can imagine that at the point x at different times there will continuously be different material points moving through. Each such material points will have a respective initial position $\hat{x}$. Thus, the velocity v at this space-time position (x,t) is still to be understood as the velocity of the material point with the initial position $\hat{x}$, i.e., $v(x,t) := d_t x(\hat{x},t) = \partial_t x$.

In an Eulerian framework the quantity of interest is written as $f(x,t)$ with x and t being anywhere within the permitted space-time continuum. Taking the total time derivative of f leads to

$$d_t f(x,t) = \partial_t f(x,t) + \nabla f(x,t)\, d_t x = \partial_t f(x,t) + v \cdot \nabla f(x,t). \tag{3.3}$$

The second term is referred to as the "transport" or "convection term". This term is a characteristic difference between the Eulerian and Lagrangian frameworks. In the Lagrangian framework, when the total time derivative is expanded into all its partial derivatives, there is no convective term due to the spatial parameter being constant in time. In contrast, in Eulerian frameworks convection can generally be expected in the expanded total time derivative.

The Eulerian framework presents itself as the natural approach for modeling fluid flow. This follows as a consequence that one is less interested in the individual behavior of particles and more interested in flow properties at certain spatial points in the flow domain. In viscous fluids with behavior similar to soft materials, a Lagrangian approach would be plausible. Generally though particle movement in fluids is considerable and their initial positions in relation to each other have effectively nothing in common with their later relative positions. Hence the Eulerian framework presents itself as the natural approach to modeling fluid flow.

The key formula for deriving the basic conservation equations in continuum mechanics is provided by Reynold's transport theorem. Let $\hat{T} : \hat{\Omega} \times I \to \Omega$ be a C^2 diffeomorphism and the scalar function $f(x,t) : \Omega \times I \to \mathbb{R}$ be differentiable. Then,

for any subset $\hat{V} \subset \hat{\Omega}$, with $V(t) = \hat{T}(\hat{V}, t)$ and the velocity field v as defined above, there holds

$$d_t \int_{V(t)} f \, dx = \int_{V(t)} \left\{ \partial_t f + \operatorname{div}(fv) \right\} dx. \tag{3.4}$$

3.3 Arbitrary Lagrangian framework

The Lagrangian and Eulerian frameworks introduced above are *natural* frameworks of references. It is more common though that one will need a framework of reference that is *arbitrary* and independent of the initial particle positions or the spatial domain. A common example (one we will later also encounter in the numerical tests) is a fluid flow in a domain that changes with time, $\Omega(t)$. Instead of modeling and simulating the flow in $\Omega(t)$ one assumes the existence of a (for a fixed time t) C^2 diffeomorphic mapping $\hat{T}(\hat{x}, t) : \hat{\Omega} \times I \to \Omega(t)$ continuous in space and time, with $\hat{\Omega}$ as the reference (and usually the initial) domain $\Omega(t)$. The requirement of C^2 diffeomorphism means that the mapping is (in addition to being diffeomorphic) also two times continuously differentiable. An approach that uses such an arbitrary frame of reference is called *"arbitrary Lagrangian-Eulerian (ALE)"*, Hughes, Liu, and Zimmermann [38]. We will also refer to an arbitrary framework as an "*ALE framework*". For an overview of the various methods of applications using an ALU framework see Bungartz and Schäfer [14] and Heil, Hazel, and Boyle [30]. With the help of the mapping $\hat{T}$ functions and operators on $\Omega(t)$ can be rewritten as such on the domain $\hat{\Omega}$. For this reason, as a preparatory measure, we introduce the most commonly needed transformation identities developed below.

By $\hat{F}$ and $\hat{J}$, we denote the Jacobian matrix and determinant of $\hat{T}$, respectively,

$$\hat{F} := \hat{\nabla} \hat{T}, \quad \hat{J} := \det \hat{F}. \tag{3.5}$$

In the context of material deformations later the mapping $\hat{T}$ will also be referred to as the *"deformation"* and accordingly $\hat{F}$ as the *"deformation gradient"*. Since $\hat{T}$ is a deformation it must for each fixed time preserve orientation and not annihilate volume. This follows from the requirement that it is continuous and diffeomorphic. Thus, $\hat{J} > 0$. Let $f(x, t)$ and $v(x, t)$ denote scalar- and vector-valued functions that are differentiable in space and time. With $\hat{T}$ we define

$$\hat{f}(\hat{x}, t) := f(\hat{T}(\hat{x}, t), t), \quad \hat{v}(\hat{x}, t) := v(\hat{T}(\hat{x}, t), t). \tag{3.6}$$

The respective reference-based spatial derivatives of $\hat{f}$ can be obtained by the chain rule,

$$\hat{\partial}_i \hat{f}(\hat{x}, t) = \sum_{j=1}^{n} \partial_j f(\hat{T}(\hat{x}), t) \, \frac{\hat{\partial} \hat{T}_j(\hat{x}, t)}{\hat{\partial} \hat{x}_i}. \tag{3.7}$$

Thus, we can write the gradient of $\hat{f}$ as

$$\hat{\nabla} \hat{f} = \nabla f \, \hat{F}. \tag{3.8}$$

For the partial and total time derivatives of a scalar function $f(x,t)$ there holds

$$\begin{aligned} \partial_t f &= \partial_t \hat{f} - (\hat{F}^{-1}\partial_t \hat{T} \cdot \nabla)\hat{f}, \\ d_t f &= \partial_t \hat{f} + (\hat{F}^{-1}(\hat{v} - \partial_t \hat{T}) \cdot \hat{\nabla})\hat{f}, \end{aligned} \tag{3.9}$$

which can be seen by considering the derivative as limit of difference quotients. Analogous relations hold for vector-valued functions.

Next, we derive transformation formulas for volume and surface integrals. Let $V \subset \Omega$ be an arbitrary volume in Ω and $\hat{V} = \hat{T}^{-1}(V)$ the corresponding subset in $\hat{\Omega}$. With $\hat{f}(\hat{x}) = f(\hat{T}(\hat{x})) = f(x)$ and $dx = \det\hat{T} d\hat{x} = \hat{J} d\hat{x}$, we transform the volume integral over V to an integral over $\hat{V}$,

$$\int_V f(x)\, dx = \int_{\hat{V}} \hat{f}(\hat{x})\hat{J}\, d\hat{x}\,. \tag{3.10}$$

The "Piola transform" of v is $\hat{J}\hat{F}^{-1}\hat{v}$. For its divergence there holds

$$\hat{J}\,\mathrm{div} v = \widehat{\mathrm{div}}(\hat{J}\hat{F}^{-1}\hat{v}), \quad x \in \hat{T}(\hat{x}) \in \Omega. \tag{3.11}$$

Further there holds

$$d_t \hat{J} = \widehat{\mathrm{div}}(\hat{J}\hat{F}^{-1}\hat{v}). \tag{3.12}$$

There hold the transformation formulas

$$\int_V \mathrm{div} v\, dx = \int_{\hat{V}} \widehat{\mathrm{div}}(\hat{J}\hat{F}^{-1}\hat{v})\, d\hat{x}. \tag{3.13}$$

and

$$\int_{\partial V} v \cdot n\, do_x = \int_{\partial \hat{V}} (\hat{J}\hat{F}^{-1}\hat{v}) \cdot \hat{n}\, d\hat{x}. \tag{3.14}$$

3.4 Conservation equations and boundary conditions

Fluid flow is modeled based on the assumption that mass, momentum, angular momentum and energy are preserved. These are naturally expressed in an Eulerian framework. Here, we will only consider "incompressible" Newtonian fluids with constant density. The constitutive relation for the (symmetric) Cauchy stress tensor in the case of an incompressible Newtonian fluid is

$$\sigma := -pI + \rho\nu(\nabla v + \nabla v^T), \tag{3.15}$$

with the kinematic viscosity ν, the hydrodynamic pressure p, the density ρ, and the flow velocity v. Conservation of angular momentum is automatically fulfilled for incompressible Newtonian fluid flow. Based on this the conservation equations for momentum and mass decouple from the energy conservation equation. For modeling our FSI problems, we will not need the temperature or the specific internal energy-density state variables and therefore omit the energy conservation equation.

Thus, we only consider the conservation equations for momentum and mass, i.e., the classical "Navier-Stokes equations":

$$\begin{aligned} \rho\partial_t v + \rho(v\cdot\nabla)v + \mathrm{div}\sigma = \rho f \quad \text{in } \Omega_f \times I, \\ \mathrm{div} v = 0 \quad \text{in } \Omega_f \times I. \end{aligned} \tag{3.16}$$

These equations are derived by using Reynold's transport theorem (3.4) for $f = \rho$ ("continuity equation") and $f = \rho v_i$ ("momentum equation").

The Navier-Stokes equations are usually not written with the full stress tensor σ in (3.15) but instead with a reduced version of the tensor $\tilde{\sigma} := -pI + \rho\nu\nabla v$, which is justified by the relation $\mathrm{div}\nabla v^T = 0$. We refrain from using the reduced tensor $\tilde{\sigma}$ since this would lead to an incorrect representation of the boundary forces. The proper calculation of these forces is most important since fluid-structure interaction is essentially driven by just these forces at the interface.

We will also need the momentum equation in an ALE framework with the respective reference frame $\hat{V}$. We use the mapping $\hat{T}$ and the notation and transformation formulas described above. There holds

$$\int_{\hat{V}} \{\hat{\rho}\hat{J}\partial_t\hat{v} + \hat{\rho}\hat{J}((\hat{v} - \partial_t\hat{T})\cdot\hat{\nabla})\hat{v} - \widehat{\mathrm{div}}(\hat{J}\sigma\hat{F}^{-T})\}\, d\hat{x} = \int_{\hat{V}} \hat{J}\hat{\rho}\hat{f}\, d\hat{x}.$$

Since this relation holds for arbitrary volumes V and respective $\hat{V}$, we conclude

$$\hat{\rho}\hat{J}\partial_t\hat{v} + \hat{\rho}\hat{J}((\hat{v} - \partial_t\hat{T})\cdot\hat{\nabla})\hat{v} - \widehat{\mathrm{div}}(\hat{J}\sigma\hat{F}^{-T}) = \hat{J}\hat{\rho}\hat{f}. \tag{3.17}$$

Generally when modeling flows using an Eulerian framework the boundaries are fixed and not moving. As a boundary condition in time an initial value v_0 for v at the initial time t_0 is prescribed. Spatially the boundary $\partial\Omega_f$ can be split into three non-overlapping parts, $\partial\Omega_f = \Gamma_{fD} \cup \Gamma_{fN} \cup \Gamma_i$ with each part relating to a different boundary condition. The first two parts are the well-known conditions

$$\begin{aligned} v = v_{fD} \quad \text{on } \Gamma_{fD} \quad \text{(Dirichlet)}, \\ \sigma n_f = g_f \quad \text{on } \Gamma_{fN} \quad \text{(Neumann)}. \end{aligned}$$

In the FSI problem there is a moving interface Γ_i which is the common boundary to the structure. We assume that on this boundary momentum is conserved and that the velocity of the fluid and material particles just at the boundary are equal. This leads to the FSI boundary conditions on Γ_i that must be fulfilled simultaneously:

$$v_f = v_s, \qquad \sigma_f n_f = \sigma_s n_f \quad \text{on } \Gamma_i. \tag{3.18}$$

Here and below, to distinguish the fluid and structure values, we have added a respective "f" or "s" suffix.

4 Variational formulations of fluid and structure problems

In this section, we prepare for the "monolithic" variational formulations of the FSI problem by developing formulations of the structure and fluid parts in the different frameworks considered.

4.1 Fluid model

For the liquid part, we assume Newtonian incompressible flow governed by the usual Navier-Stokes equations, i.e., the equations describing conservation of mass and momentum. The (constant) density and kinematic viscosity of the fluid are ρ_f and ν_f, respectively.

4.1.1 Fluid model in Eulerian formulation

The equations are written in an Eulerian framework in the time-dependent domain $\Omega_f(t)$. The physical unknowns are the scalar pressure field $p_f \in \mathcal{L}_f$ and the vector velocity field $v_f \in v_f^D + \mathcal{V}_f^0$. Here, v_f^D is a suitable extension of the prescribed Dirichlet data on the boundaries (both moving or stationary) of Ω_f, and g_1 is a suitable extension to all of $\partial\Omega_f$ of the Neumann data for $\sigma_f \cdot n$ on the boundaries. We have "hidden" the fluid-structure interface conditions of continuity of velocity and normal stress in parts of the boundary data v_f^D and g_1.

The variational form of the Navier-Stokes equations in an Eulerian framework is obtained by multiplying them with suitable test functions from the test space V_f^0 for the momentum equations and L_f for the mass conservation equation.

Problem 1 (Fluid model in Eulerian formulation)**.** *Find* $\{v_f, p_f\} \in \{v_f^D + \mathcal{V}_f^0\} \times \mathcal{L}_f$, *such that* $v_f(0) = v_f^0$, *and*

$$\begin{aligned} (\rho_f(\partial_t + v_f \cdot \nabla)v_f, \psi^v)_f + (\sigma_f, \varepsilon(\psi^v))_f &= (g_1, \psi^v)_{\partial\Omega_f} + (f, \psi^v)_f, \\ (\mathrm{div} v_f, \psi^p)_f &= 0, \end{aligned} \tag{4.1}$$

for all $\{\psi^v, \psi^p\} \in V_f^0 \times L_f$, *where*

$$\sigma_f := -p_f I + 2\rho_f \nu_f \varepsilon(v_f), \quad \varepsilon(v) := \tfrac{1}{2}(\nabla v + \nabla v^T).$$

4.1.2 Fluid model in ALE formulation

In fluid-structure interaction problems that we will later be observing the FSI domain Ω is time independent, but it is composed of the fluid domain Ω_f and the structure domain Ω_s, which will be changing with time. An approach to modeling a fluid flow in a dynamic domain is assuming that a reference domain $\hat{\Omega}_f$ and piecewise continuously differentiable invertible mapping $\hat{T}$ exist so that $\hat{T}(\hat{x}, t) : \hat{\Omega}_f \times I \to \Omega(t)$. Based on this assumption, we rewrite the Navier-Stokes equations in an ALE framework with the reference frame $\hat{\Omega}_f$ where we use the mapping $\hat{T}$ and the notation described above,

$$\begin{aligned} \hat{J}\rho\partial_t\hat{v} + \hat{J}\rho(\hat{F}^{-1}(\hat{v} - \partial_t\hat{T}) \cdot \hat{\nabla})\hat{v} - \widehat{\mathrm{div}}(\hat{J}\hat{\sigma}\hat{F}^{-T}) &= \hat{J}\rho\hat{f} \quad \text{in } \hat{\Omega}_f, \\ \widehat{\mathrm{div}}(\hat{J}\hat{F}^{-1}\hat{v}) &= 0 \quad \text{in } \hat{\Omega}_f, \end{aligned} \tag{4.2}$$

with $\hat{\sigma} := -\hat{p}I + \rho\nu(\hat{\nabla}\hat{v}\hat{F}^{-1} + \hat{F}^{-T}\hat{\nabla}\hat{v}^T)$, $\hat{F} := \hat{\nabla}\hat{T}$, and $\hat{J} := \det\hat{F}$.

Similarly the boundary conditions must be set in the ALE framework. As a boundary condition in time the same initial value is prescribed $\hat{v}_0(\hat{x}, 0) = v_0(\hat{T}(\hat{x}, 0)) =$

v_0 for $\hat{v}$, now set in the ALE framework, at the initial time t_0. The fluid boundary $\partial\hat{\Omega}_f$ can be split into three non-overlapping components, $\partial\hat{\Omega}_f = \hat{\Gamma}_{fD} \cup \hat{\Gamma}_{fN} \cup \hat{\Gamma}_i$, with each part relating to a different boundary condition. The first two parts are the well-known conditions

$$\begin{aligned} \hat{v} &= \hat{v}_D \quad \text{on } \hat{\Gamma}_{fD} \quad \text{(Dirichlet)}, \\ \hat{J}\hat{\sigma}\hat{F}^{-T}\hat{n} &= \hat{g} \quad \text{on } \hat{\Gamma}_{fN} \quad \text{(Neumann)}. \end{aligned}$$

The moving boundary Γ_i corresponds to a fixed boundary $\hat{\Gamma}_i$ on the reference domain. In an Eulerian framework the boundary conditions on the moving boundary Γ_i are the same as in the fluid flow case: continuity of velocity and normal-flux of the stress. In the reference configuration the velocity is not transformed. The stress though is transformed, since not the Cauchy stress tensor is used in the momentum conservation equations, but instead the first Piola-Kirchhoff stress tensor. This leads to the boundary conditions

$$\hat{v}_f = \hat{v}_s, \qquad \hat{J}_f\hat{\sigma}_f\hat{F}_f^{-T}\hat{n}_f = \hat{J}_s\hat{\sigma}_s\hat{F}_s^{-T}\hat{n}_f \quad \text{on } \hat{\Gamma}_i. \tag{4.3}$$

The variational form of the Navier-Stokes equations in an ALE framework is again obtained by multiplying them with suitable test functions from the test space $\hat{V}_f^0$ for the momentum equations and $\hat{L}_f$ for the mass conservation equation. For later purposes, we write all fluid specific variables with a respective "f" suffix. This includes the domain mapping now referred to as $\hat{T}_f$. The physical unknowns are the scalar pressure $\hat{p}_f \in \hat{\mathcal{L}}_f$ and the velocity $\hat{v}_f \in \hat{v}_f^D + \hat{\mathcal{V}}_f$.

Problem 2 (Fluid model in ALE formulation)**.** *Find* $\{\hat{v}_f, \hat{p}_f\} \in \{\hat{v}_f^D + \hat{\mathcal{V}}_f^0\} \times \hat{\mathcal{L}}_f$ *such that* $\hat{v}_f(0) = \hat{v}_f^0$ *and*

$$\begin{aligned} &(\hat{J}_f\rho_f\partial_t\hat{v}_f + \hat{J}_f\rho_f(\hat{F}_f^{-1}(\hat{v}_f - \partial_t\hat{T}_f)\cdot\hat{\nabla})\hat{v}_f, \hat{\psi}^v)_{\hat{f}} + (\hat{J}_f\hat{\sigma}_f\hat{F}_f^{-T}, \hat{\nabla}\hat{\psi}^v)_{\hat{f}} \\ &\qquad = (\hat{g}_f, \hat{\psi}^v)_{\hat{\Gamma}_{fN}} + (\hat{J}_f\hat{\sigma}_f\hat{F}_f^{-T}\hat{n}_f, \hat{\psi}^v)_{\hat{\Gamma}_i} + (\rho_f\hat{J}_f\hat{f}_f, \hat{\psi}^v)_{\hat{f}}, \qquad (4.4) \\ &(\widehat{\mathrm{div}}(\hat{J}_f\hat{F}_f^{-1}\hat{v}_f, \hat{\psi}^p)_{\hat{f}} = 0, \end{aligned}$$

for all $\{\hat{\psi}^v, \hat{\psi}^p\} \in \hat{V}_f^0 \times \hat{L}_f$ *where*

$$\hat{\sigma}_f := -\hat{p}_f I + \rho_f\nu_f(\hat{\nabla}\hat{v}_f\hat{F}_f^{-1} + \hat{F}_f^{-T}\hat{\nabla}\hat{v}_f^T), \quad \hat{F}_f := \hat{\nabla}\hat{T}_f, \quad \hat{J}_f := \det\hat{F}_f.$$

Here, $\hat{v}_f^D$ is a suitable extension of the prescribed Dirichlet data on the boundaries of $\hat{\Omega}_f$ and $\hat{g}_f$ is the Neumann boundary condition on $\hat{\Gamma}_{fN}$. We have hidden the fluid-structure interface condition of continuity of velocity in part of the boundary data $\hat{v}_f^D$. The fluid-structure interface condition of continuity of the force $\hat{J}_f\hat{\sigma}\hat{F}^{-T}\hat{n}_f$, we have let stand for later purposes.

4.2 Structure model

Material deformations are modeled based on the assumption of conservation of momentum and optionally volume. The main quantity of interest is the vector field

describing the displacement of the body from its initial state. Consequently the Lagrangian formulation is the natural frame of reference. Here, we will consider elastic materials, that is to say the observed material returns to its initial state once all applied forces are removed. We refer to the domain of the initial state as $\hat{\Omega}_s$ ("reference configuration") and use the mapping $\hat{T}$ and the notation introduced above. The displacement $\hat{u}$ and mapping $\hat{T}$ ("deformation") satisfy the relation

$$\hat{T}(\hat{x},t) = \hat{x} + \hat{u}(\hat{x},t). \tag{4.5}$$

The gradient of $\hat{T}$ is the deformation gradient $\hat{F} = \hat{\nabla}\hat{T} = I + \hat{\nabla}\hat{u}$. The state variables are the density $\hat{\rho}$ in the initial state, the velocity $\hat{v}$, the displacement $\hat{u}$, and the Cauchy stress tensor $\hat{\sigma}$, which is a function of $\hat{u}$ and optionally a pressure $\hat{p}$. The external force is denoted by $\hat{f}$.

In the examples presented below, we consider two different types of materials, a standard compressible elastic material described by the "St. Venant-Kirchhoff (STVK)" model and an "incompressible neo-Hookean (INH)" material. These two models will be described in the next two subsections.

The density of the structure is ρ_s. The material elasticity is usually described by a set of two parameters, the Poisson ration ν_s and the Young modulus E_s, or alternatively, the Lamé coefficients λ_s and μ_s. These parameters satisfy the following relations:

$$\begin{aligned} \nu_s &= \frac{\lambda_s}{2(\lambda_s+\mu_s)}, \quad E_s = \mu_s\frac{3\lambda_s+2\mu_s}{\lambda_s+\mu_s}, \\ \mu_s &= \frac{E_s}{2(1+\nu_s)}, \quad \lambda_s = \frac{\nu_s E_s}{(1+\nu_s)(1-2\nu_s)}, \end{aligned}$$

where $\nu_s = \frac{1}{2}$ for incompressible and $\nu_s < \frac{1}{2}$ for compressible material. Common notation for the stress tensor and various constituents are $P := \hat{J}\hat{\sigma}\hat{F}^{-T}$ and $S := \hat{F}^{-1}P$ for the "1st and 2nd Piola-Kirchhoff stress tensor", $\hat{E} := \frac{1}{2}(\hat{F}^T\hat{F} - I)$ for the "Green-Lagrange strain tensor", and $\hat{F}\hat{F}^T$ and $\hat{F}^T\hat{F}$ for the "left and right Cauchy-Green deformation tensor". We encounter the 1st Piola-Kirchhoff stress tensor as the "transformed" stress tensor on the reference domain $\hat{\Omega}$.

Principally the momentum conservation equations here are the same as with fluid flows, the only differences are that they are commonly set in a Lagrangian framework and the constitutive equation for the Cauchy stress tensor is based on the displacement field and not the velocity field. The equations for the elastic materials below differ slightly due to the different constitutive laws for the stress tensor.

Generally when modeling material deformation the boundaries will be moving in time. In the Lagrangian framework boundary conditions can be posed in the reference configuration. As a boundary condition in time initial values $\hat{u}^0$ and $\hat{v}^0$ for $\hat{u}$ and $\hat{v}$ are prescribed at the initial time t_0. Similar to the fluid boundary conditions the material boundary $\partial\hat{\Omega}_s$ can be split into three non-overlapping components, $\partial\hat{\Omega}_s = \hat{\Gamma}_{sD} \cup \hat{\Gamma}_{sN} \cup \hat{\Gamma}_i$, with each part relating to a different boundary condition. The first two parts are the well-known conditions

$$\begin{aligned} \hat{u} = \hat{u}^D, \quad \hat{v} = \hat{v}^D \quad \text{on } \hat{\Gamma}_{sD} \quad \text{(Dirichlet)}, \\ \hat{J}\hat{\sigma}\hat{F}^{-T}\hat{n} = \hat{g} \quad \text{on } \hat{\Gamma}_{sN} \quad \text{(Neumann)}. \end{aligned}$$

Here, $\hat{u}^D$ and $\hat{v}_s^D$ are assumed to be given as suitable extensions of the prescribed Dirichlet data on the boundaries of $\hat{\Omega}_s$, and $\hat{g}_2$ is a suitable extension to all of $\partial\hat{\Omega}_s$ of the Neumann data for $\hat{\sigma}_s \cdot n$ on the boundaries. For the sake of simplicity, we assume that the only boundary displacement that take place are on $\hat{\Gamma}_i$, i.e.,

$$\hat{u}^D = \hat{v}_s^D = 0 \text{ on } \partial\hat{\Omega}_s \setminus \hat{\Gamma}_i. \tag{4.6}$$

The moving boundary $\hat{\Gamma}_i$ is of course fixed on the reference domain. We assume that an appropriate mapping of the initial fluid domain $\hat{\Omega}_f$ on the present domain Ω_f is provided. With this in mind, we can rewrite the fluid quantities v and σ in an ALE framework. In an Eulerian framework the boundary conditions on the moving boundary Γ_i are the same as in the fluid flow case: continuity of velocity v and the normal-flux of the stress σn. In the reference configuration the velocity is not transformed. The stress though is transformed since not the Cauchy stress tensor is used in the momentum equations but instead the 1st Piola-Kirchhoff stress tensor. This leads to the boundary conditions

$$\hat{v}_s = \hat{v}_f, \qquad \hat{J}_s\hat{\sigma}_s\hat{F}_s^{-T}\hat{n}_s = \hat{J}_f\hat{\sigma}_f\hat{F}_f^{-T}\hat{n}_s \quad \text{on } \hat{\Gamma}_i. \tag{4.7}$$

Similar to the structure variables the fluid variables are also denoted with a "hat" , which indicates that they are set in an ALE framework. Again, similarly as for the fluid problem, we will hide the fluid-structure interface conditions of continuity of velocity and normal stress in parts of the boundary data $\hat{v}_s^D$ and $\hat{g}_2$.

4.2.1 St. Venant-Kirchhoff (STVK) material

The St. Venant-Kirchhoff (STVK) model is a classical (geometrically) nonlinear model for compressible elastic materials. It can be used for large displacements but requires small strains $\hat{E}$. This model is governed by the equations for conservation of mass and momentum. Again these equations are written in Lagrangian form using the same notation as above. The sought unknowns are the displacement $\hat{u}$ and the velocity $\hat{v}$, which are determined by the following system:

$$\begin{aligned} \hat{\rho}d_t\hat{v} - \widehat{\mathrm{div}}(\hat{J}\hat{\sigma}\hat{F}^{-T}) &= \hat{\rho}\hat{f} \quad \text{in } \hat{\Omega}_s, \\ d_t\hat{u} - \hat{v} &= 0 \quad \text{in } \hat{\Omega}_s, \end{aligned} \tag{4.8}$$

where $\hat{F} := I + \hat{\nabla}\hat{u}_s$, $\hat{J} := \det\hat{F}$, $\hat{E} := \frac{1}{2}(\hat{F}^T\hat{F} - I)$, and

$$\hat{\sigma} = \hat{J}^{-1}\hat{F}(\lambda_s(\mathrm{tr}\hat{E})I + 2\mu_s\hat{E})\hat{F}^T.$$

The variational formulation is as follows.

Problem 3 (STVK structure model in Lagrangian formulation)**.** *Find* $\{\hat{u}_s, \hat{v}_s\} \in \{\hat{u}^D + \hat{\mathcal{V}}_s^0\} \times \{\hat{v}_s^D + \hat{\mathcal{V}}_s^0\}$*, such that* $\hat{u}_s(0) = \hat{u}_s^0$, $\hat{v}_s(0) = \hat{v}_s^0$, *and*

$$\begin{aligned} (\rho_s d_t\hat{v}_s, \hat{\psi}^u)_{\hat{s}} + (\hat{J}\ \hat{\sigma}_s\ \hat{F}^{-T}, \hat{\varepsilon}(\hat{\psi}^u))_{\hat{s}} &= (\hat{g}_2, \hat{\psi}^u)_{\partial\hat{\Omega}_s} + (\hat{f}_2, \hat{\psi}^u)_{\hat{s}}, \\ (d_t\hat{u}_s - \hat{v}_s, \hat{\psi}^v)_{\hat{s}} &= 0, \end{aligned} \tag{4.9}$$

for all $\{\hat{\psi}^u, \hat{\psi}^v\} \in \hat{V}_s^0 \times \hat{V}_s^0$, *where* $\hat{\varepsilon}(\hat{\psi}^u) := \frac{1}{2}(\hat{\nabla}\hat{\psi}^u + \hat{\nabla}\hat{\psi}^{uT})$.

4.2.2 Incompressible Neo-Hookean (INH) material

Numerous materials can be subjected to strains without a notable change of volume. Typical examples of such materials are plastics and rubber-like substances. A common idealization in continuum mechanics is to regard such materials as generally "incompressible" that only permit so-called "isochoric" deformations. The incompressibility of the material is ensured by demanding that the deformation conserve volume, hence the additional constraint $\hat{J} = 1$. The sought unknowns are the displacement $\hat{u}$, the velocity $\hat{v}$, and the (hydrostatic) pressure $\hat{p}$, which are determined by the system

$$\begin{aligned} \hat{\rho} d_t \hat{v} - \widehat{\mathrm{div}}(\hat{\sigma}\hat{F}^{-T}) &= \hat{\rho}\hat{f}, \quad \text{in } \hat{\Omega}_s, \\ d_t \hat{u} - \hat{v} &= 0 \quad \text{in } \hat{\Omega}_s, \\ \hat{J} - 1 &= 0 \quad \text{in } \hat{\Omega}_s, \end{aligned} \tag{4.10}$$

with $\hat{\sigma} = -\hat{p}I + \mu_s(\hat{F}\hat{F}^T - I)$ and $\hat{F} = I + \hat{\nabla}\hat{u}$.

With suitable function spaces $\hat{\mathcal{V}}_s^0$ for the vector displacement and velocity fields and $\hat{\mathcal{L}}_s$ for the scalar pressure field $\hat{p}_s$, we write these equations in the following variational form.

Problem 4 (INH structure model in Lagrangian formulation)**.** *Find* $\{\hat{u}_s, \hat{v}_s, \hat{p}_s\} \in \{\hat{u}^D + \hat{\mathcal{V}}_s^0\} \times \{\hat{v}_s^D + \hat{\mathcal{V}}_s^0\} \times \hat{\mathcal{L}}_s$*, such that* $\hat{u}_s(0) = \hat{u}_s^0$, $\hat{v}_s(0) = \hat{v}_s^0$, *and*

$$\begin{aligned} (\rho_s d_t \hat{v}_s, \hat{\psi}^u)_{\hat{s}} + (\hat{\sigma}_s \hat{F}^{-T}, \hat{\varepsilon}(\hat{\psi}^u))_{\hat{s}} &= (\hat{g}_2, \hat{\psi}^u)_{\partial\hat{\Omega}_s} + (\hat{f}_2, \hat{\psi}^u)_{\hat{s}}, \\ (d_t \hat{u}_s - \hat{v}_s, \hat{\psi}^v)_{\hat{s}} &= 0, \\ (\det\hat{F}, \hat{\psi}^p)_{\hat{s}} &= (1, \hat{\psi}^p)_{\hat{s}}, \end{aligned} \tag{4.11}$$

for all $\{\hat{\psi}^u, \hat{\psi}^v, \hat{\psi}^p\} \in \hat{V}_s^0 \times \hat{V}_s^0 \times \hat{L}_s$, *where* $\hat{F} := I + \hat{\nabla}\hat{u}_s$ *and*

$$\hat{\sigma}_s := -\hat{p}_s I + \mu_s(\hat{F}\hat{F}^T - I), \quad \hat{\varepsilon}(\hat{\psi}^u) := \tfrac{1}{2}(\hat{\nabla}\hat{\psi}^u + \hat{\nabla}\hat{\psi}^{uT}).$$

4.2.3 Structure model in Eulerian framework

In fluid-structure interaction problems the FSI domain Ω is usually time independent but it is composed of the fluid domain Ω_f and the structure domain Ω_s, which are be changing with time. One approach, already mentioned, to treating this problem is to introduce a mapping $\hat{T}(\hat{x}, t) : \hat{\Omega} \times I \to \Omega(t)$. With this mapping the fluid problem is rewritten in an ALE framework. As an alternative one may change the reference frame of the structure from Lagrangian to Eulerian which will eventually lead to a fully Eulerian formulation of the whole FSI problem.

All material stress quantities occurring above are based on the Lagrangian deformation gradient $\hat{F} := I + \hat{\nabla}\hat{u}$. In an Eulerian framework, we will still have the deformation since this is simply a quantity being specified in another reference frame, i.e., $u(x) = \hat{u}(\hat{x})$. What is not immediately available though is the deformation gradient $\hat{\nabla}\hat{u}$ since $\hat{\nabla}\hat{u} \neq \nabla u$. Therefore, we introduce the "inverse deformation"

$$T(x, t) : \Omega_s(t) \times I \to \hat{\Omega}_s, \quad T(x, t) := \hat{x} = x - u(x, t).$$

Together with the deformation $\hat{T}(\hat{x},t)$ this leads to the identity

$$T(\hat{T}(\hat{x},t),t) = \hat{x}.$$

Differentiating this with respect to $\hat{x}$ gives us $(I-\nabla u)(I+\widehat{\nabla}\hat{u}) = I$ or $(I+\hat{\nabla}\hat{u}) = (I-\nabla u)^{-1}$, and, thus,

$$\widehat{\nabla}\hat{u} = (I-\nabla u)^{-1} - I. \tag{4.12}$$

Hence the gradients and Jacobi determinants of the deformation and inverse deformation relate to each other in the following manner:

$$F := I - \nabla u = \hat{F}^{-1}, \quad J := \det F = \det\hat{F}^{-1} = \hat{J}^{-1}. \tag{4.13}$$

The total time derivatives of the velocity and displacement are in the usual way written as

$$d_t v = \partial_t v + v\cdot\nabla v, \quad d_t u = \partial_t u + v\cdot\nabla u.$$

Using the above relations, we can rewrite the structure equations for St. Venant-Kirchhoff (STVK) materials and incompressible neo-Hookean (INH) materials in Eulerian framework. The unknowns are the displacement u, the velocity v and in the INH case the (hydrostatic) pressure p, which are determined by the following system:

$$\begin{aligned} \hat{\rho}J\partial_t v + \hat{\rho}Jv\cdot\nabla v - \mathrm{div}\sigma &= \hat{\rho}Jf \quad \text{in } \Omega_s, \\ \partial_t u + v\cdot\nabla u - v &= 0 \quad \text{in } \Omega_s, \\ 1 - J &= 0 \quad \text{in } \Omega_s \quad \text{(INH material)}, \end{aligned} \tag{4.14}$$

where $E := \frac{1}{2}(F^{-T}F^{-1} - I)$, $F := I - \nabla u$, $J := \det F$, and

$$\sigma := \begin{cases} JF^{-1}(\lambda_s \mathrm{tr}E\, I + 2\mu_s E)F^{-T} & \text{(STVK material)}, \\ -pI + \mu_s(F^{-1}F^{-T} - I) & \text{(INH material)}. \end{cases}.$$

Similarly the boundary conditions must be set in the Eulerian framework. As a boundary condition in time the same initial value v^0, now in Eulerian framework, is prescribed for v at the initial time t_0. The fluid boundary $\partial\Omega_s$ is again split into three non-overlapping components $\partial\Omega_s = \Gamma_{sD}\cup\Gamma_{sN}\cup\Gamma_i$, with each part relating to a different boundary condition,

$$\begin{aligned} v &= v^D \quad \text{on } \Gamma_{sD} \quad \text{(Dirichlet)}, \\ \sigma n &= g \quad \text{on } \Gamma_{sN} \quad \text{(Neumann)}. \end{aligned}$$

The fixed boundary $\hat{\Gamma}_i$ on the reference domain now becomes the moving boundary Γ_i just as in the fluid flow case. The boundary conditions on Γ_i are similar to the fluid flow case: continuity of velocity v and the normal flux of the stress σn,

$$v_s = v_f, \quad \sigma_s n_s = \sigma_f n_s \quad \text{on } \Gamma_i. \tag{4.15}$$

Just as in the Lagrangian framework u_s^D and v_s^D are suitable extensions of the prescribed Dirichlet data on the boundaries of Ω_s, and g_s is the Neumann boundary condition on Γ_{sN}. Similarly as for the fluid problems, we have hidden the fluid-structure coupling condition of continuity of velocity in part of the boundary data v_s^D. The condition of continuity of normal stresses $\sigma_s n_s$, we have let stand.

The variational form of the structure equations in an Eulerian framework is again obtained by multiplying them with suitable test functions from the test space V_s^0 for the momentum equations and L_s for velocity/displacement and the optional incompressibility equations. The equations are written in an Eulerian framework in the domain Ω_s. The physical unknowns are the displacement $u_s \in u_s^D + \mathcal{V}_s^0$, the velocity $v_s \in v_s^D + \mathcal{V}_s^0$, and the optional pressure $p_s \in \mathcal{L}_s$, which are determined by the following problem.

Problem 5 (Structure model in Eulerian formulation)**.** *Find* $\{u_s, v_s\} \in \{u_s^D + \mathcal{V}_s^0\} \times \{v_s^D + \mathcal{V}_s^0\}$ *and, in the INH case,* $p_s \in \mathcal{L}_s$*, such that* $u_s(0) = u_s^0$*,* $v_s(0) = v_s^0$*, and*

$$\begin{aligned} (\hat{\rho}_s J_s \partial_t v_s, \psi^v)_s + (\hat{\rho}_s J_s v_s \cdot \nabla v_s, \psi^v)_s + (\sigma_s, \nabla \psi^v)_s \\ = (g_s, \psi^v)_{\Gamma_{sN}} + (\sigma_s n_s, \psi^v)_{\Gamma_i} + (\hat{\rho}_s J_s f_s, \psi^v)_s, \\ (\partial_t u_s + v_s \cdot \nabla u_s - v_s, \psi^u)_s = 0, \\ (1 - \det F_s, \psi^p) = 0 \quad \textit{(in the INH case)}, \end{aligned} \tag{4.16}$$

for all $\{\psi^u, \psi^v\} \in V_s^0 \times V_s^0$ *and, in the INH case,* $\psi^p \in L_s$ *where* $F_s := I - \nabla u_s$*,* $J_s := \det F_s$*,* $E := \frac{1}{2}(F_s^{-T} F_s^{-1} - I)$*, and*

$$\sigma_s := \begin{cases} J_s F_s^{-1} (\lambda_s \mathrm{tr} E\, I + 2\mu_s E) F_s^{-T} & \textit{(in the STVK case)}, \\ -p_s I + \mu_s (F_s^{-1} F_s^{-T} - I) & \textit{(in the INH case)}. \end{cases}$$

5 Variational formulations of the FSI problem

Based on the foregoing preparations, we can now state the variational formulations of the FSI problem in the ALE and the fully Eulerian frameworks.

5.1 The ALE formulation of the FSI problem

The ALE formulation of the FSI problem uses the natural Lagrangian framework for the structure and the fluid model is transformed from its Eulerian description into an arbitrary Lagrangian framework. Accordingly, the variational ALE formulation of the fluid part is stated on the (arbitrary) reference domain $\hat{\Omega}_f$, while the structure part uses the domain $\hat{\Omega}_s$, where $\hat{\Omega} = \hat{\Omega}_f \cup \hat{\Gamma}_i \cup \hat{\Omega}_s$ forms the common reference domain. In this setting the continuity of velocity across the fluid-structure interface $\hat{\Gamma}_i$ is strongly enforced by requiring one common continuous field for the velocity on $\hat{\Omega}$. The stress interface condition

$$\hat{J}_f \hat{\sigma}_f \hat{F}_f^{-T} \hat{n}_f = \hat{J}_s \hat{\sigma}_s \hat{F}_s^{-T} \hat{n}_f \quad \text{on } \hat{\Gamma}_i,$$

is still present in the form of a jump of the 1st Piola-Kirchhoff normal stresses of both subsystems,

$$(\hat{J}_f \hat{\sigma}_f \hat{F}_f^{-T} \hat{n}_f, \hat{\psi}^v)_{\hat{\Gamma}_i} + (\hat{J}_s \hat{\sigma}_s \hat{F}_s^{-T} \hat{n}_f, \hat{\psi}^v)_{\hat{\Gamma}_i},$$

on the right hand side. By omitting these integral terms the continuity of the normal stress becomes imposed "weakly", i.e., a condition implicitly contained in the combined variational formulation.

The combined formulation though implies that a domain mapping function $\hat{T}_f$ for the fluid domain is known. Such a mapping is obtained by adding an auxiliary equation to the fluid and structure equations. The boundary conditions for this mapping are clear: There is no deformation on all "outer" boundaries $\partial\hat{\Omega}_f \setminus \hat{\Gamma}_i$, and the deformation on $\hat{\Gamma}_i$ should be equal to $\hat{u}_s$. Thus, the global deformation $\hat{u}$ with $\hat{u}|_{\hat{\Omega}_s} = \hat{u}_s$ must have a trace on $\hat{\Gamma}_i$ such that $\hat{u} \in \hat{u}^D + \hat{\mathcal{V}}^0$.

The deformation itself can be sought as the solution to various "deformation problems" (i.e., "extension problems" of the boundary data $\hat{u}|_{\hat{\Omega}_s} = \hat{u}_s$), the simplest being the harmonic extension. If it is necessary that the deformation preserves volume an incompressibility condition can be added in the form

$$\hat{J}_f = \det(I + \widehat{\nabla}\hat{u}_s) = 1, \tag{5.1}$$

or in a simplified form $\widehat{\mathrm{div}}\hat{u}_s = 0$, leading to the "Stokes extension". If the deformation should be more "smooth", then as an alternative the biharmonic extension can be used. In what follows, we use the harmonic extension of the structure displacement $\hat{u}_s$ into the fluid domain.

The remaining parts of the Neumann data $\hat{g}_f$ and $\hat{g}_s$ form the Neumann boundary data on $\hat{\Gamma}_N := \hat{\Gamma}_{fN} \cup \hat{\Gamma}_{sN}$ and are combined to $\hat{g}$. The right hand side functions $\hat{f}_f$ and $\hat{f}_s$ are combined to $\hat{f}$. We define the density $\hat{\rho}$ and the Cauchy stress tensor $\hat{\sigma}$ for the whole domain by

$$\hat{\rho}(\hat{x}) := \begin{cases} \hat{\rho}_f(\hat{x}), & \hat{x} \in \hat{\Omega}_f, \\ \hat{\rho}_s(\hat{x}), & \hat{x} \in \hat{\Omega}_s \cup \Gamma_i, \end{cases} \qquad \hat{\sigma}(\hat{x}) := \begin{cases} \hat{\sigma}_f(\hat{x}), & \hat{x} \in \hat{\Omega}_f, \\ \hat{\sigma}_s(\hat{x}), & \hat{x} \in \hat{\Omega}_s \cup \Gamma_i. \end{cases} \tag{5.2}$$

Further, we introduce the characteristic functions $\hat{\chi}_f$ and $\hat{\chi}_s$ defined by

$$\hat{\chi}_f(\hat{x}) := \begin{cases} 1, & \hat{x} \in \hat{\Omega}_f, \\ 0, & \hat{x} \in \hat{\Omega}_s \cup \hat{\Gamma}_i, \end{cases} \qquad \hat{\chi}_s := 1 - \hat{\chi}_f. \tag{5.3}$$

With this notation the variational ALE formulations of the nonstationary as well as the stationary FSI problem read as follows.

Problem 6 (ALE formulation of FSI problem)**.** *Find* $\{\hat{v}, \hat{p}, \hat{u}\} \in \{\hat{v}^D + \hat{\mathcal{V}}^0\} \times \hat{\mathcal{L}} \times \{\hat{u}^D + \hat{\mathcal{V}}^0\}$*, such that* $\hat{v}(0) = \hat{v}^0$*,* $\hat{u}(0) = \hat{u}^0$*, and*

$$\begin{aligned} &(\hat{\chi}_s\hat{\rho}d_t\hat{v}, \hat{\psi}^v) + (\hat{\chi}_f\hat{J}\hat{\rho}(\partial_t\hat{v} + ((\hat{F}^{-1}(\hat{v} - \partial_t\hat{T}) \cdot \widehat{\nabla})\hat{v}, \hat{\psi}^v) \\ &\qquad + (\hat{J}\hat{\sigma}\hat{F}^{-T}, \widehat{\nabla}\hat{\psi}^v) = (\hat{g}, \hat{\psi}^v)_{\hat{\Gamma}_N} + (\hat{\rho}\hat{J}\hat{f}, \hat{\psi}^v), \\ &(\hat{\chi}_f\widehat{\mathrm{div}}(\hat{J}\hat{F}^{-1}\hat{v}), \hat{\psi}^p) + \hat{\alpha}_p\{(\hat{\chi}_s\widehat{\nabla}\hat{p}, \widehat{\nabla}\hat{\psi}^p) - (\hat{\partial}_n\hat{p}, \hat{\psi}^p)_{\hat{\Gamma}_i}\} = 0, \quad \textit{(STVK)} \\ &\qquad (\hat{\chi}_f\widehat{\mathrm{div}}(\hat{J}\hat{F}^{-1}\hat{v}), \hat{\psi}^p) + (\hat{\chi}_s(\hat{J} - 1), \hat{\psi}^p) = 0, \quad \textit{(INH)} \\ &(\hat{\chi}_s(d_t\hat{u} - \hat{v}), \hat{\psi}^u) + \hat{\alpha}_u\{(\hat{\chi}_f\widehat{\nabla}\hat{u}, \widehat{\nabla}\hat{\psi}^u) - (\hat{\partial}_n\hat{u}, \hat{\psi}^u)_{\hat{\Gamma}_i}\} = 0, \end{aligned} \tag{5.4}$$

for all $\{\hat\psi^v,\hat\psi^p,\hat\psi^u\}\in\hat V^0\times\hat L^*\times\hat V^0$ *, where* $\hat\alpha_p,\hat\alpha_u$ *are small positive constants,* $\hat T:=\mathrm{id}+\hat u$ *,* $\hat F:=\widehat\nabla\hat T$ *,* $\hat J:=\det\hat F$ *, and*

$$\hat\sigma|_{\hat\Omega_f}:=-\hat pI+\rho_f\nu_f(\widehat\nabla\hat v\hat F^{-1}+\hat F^{-T}\widehat\nabla\hat v^T),$$
$$\hat\sigma|_{\hat\Omega_s}:=\begin{cases}\hat J^{-1}\hat F(\lambda_s\mathrm{tr}\hat E\,I+2\mu_s\hat E)\hat F^T & \textit{(STVK)},\\ -\hat pI+\mu_s(\hat F\hat F^T-I), & \textit{(INH)}.\end{cases}$$

Problem 7 (ALE formulation of stationary FSI problem)**.** *Find* $\{\hat v,\hat p,\hat u\}\in\{\hat v^D+\hat V^0\}\times\hat L\times\{\hat u^D+\hat V^0\}$ *, such that*

$$\begin{aligned}(\hat\chi_f\hat J\hat\rho\hat F^{-1}\hat v\cdot\widehat\nabla)\hat v,\hat\psi^v)+(\hat J\hat\sigma\hat F^{-T},\widehat\nabla\hat\psi^v)&=(\hat g,\hat\psi^v)_{\hat\Gamma_N}+(\hat\rho\hat J\hat f,\hat\psi^v),\\ (\hat\chi_f\widehat{\mathrm{div}}(\hat J\hat F^{-1}\hat v),\hat\psi^p)+\hat\alpha_p\big\{(\hat\chi_s\widehat\nabla\hat p,\widehat\nabla\hat\psi^p)-(\partial_n\hat p,\hat\psi^p)_{\hat\Gamma_i}\big\}&=0,\quad\textit{(STVK)}\\ (\hat\chi_f\widehat{\mathrm{div}}(\hat J\hat F^{-1}\hat v),\hat\psi^p)+(\hat\chi_s(\hat J-1),\hat\psi^p)&=0,\quad\textit{(INH)}\\ -(\hat\chi_s\hat v,\hat\psi^u)+\hat\alpha_u\big\{(\hat\chi_f\widehat\nabla\hat u,\widehat\nabla\hat\psi^u)-(\hat\partial_n\hat u,\hat\psi^u)_{\hat\Gamma_i}\big\}&=0,\end{aligned}\tag{5.5}$$

for all $\{\hat\psi^v,\hat\psi^p,\hat\psi^u\}\in\hat V^0\times\hat L\times\hat V^0$ *, where* $\hat\alpha_p,\hat\alpha_u$ *are small positive constants, and all other quantities are as defined in Problem 6.*

5.2 The fully Eulerian formulation of the FSI problem

The variational Eulerian formulation of the fluid problem is posed on the domain Ω_f , while the corresponding formulation of the structure problem is posed on the domain Ω_s . By construction the fluid-structure interaction interface Γ_i of both problems match. Now, both problems are combined into one complete problem on the combined domain $\Omega=\Omega_f\cup\Gamma_i\cup\Omega_s$.

Again, exactly as in the ALE formulation described above, continuity of the velocity across the fluid-structure interface Γ_i is strongly enforced by requiring one common continuous field for the velocity on Ω . The stress interface condition $\sigma_f n_f=\sigma_s n_f$ on Γ_i is still present in the form of a jump of the Cauchy stresses of both systems

$$([\sigma\cdot n],\psi^v)_{\Gamma_i}=(\sigma_f n_f,\psi^v)_{\Gamma_i}+(\sigma_s n_s,\psi^v)_{\Gamma_i}$$

on the right hand side. By omitting this boundary integral jump the (weak) continuity of the normal stress becomes an implicit condition of the combined variational formulation.

The remaining parts of the Neumann data g_f and g_s now form the Neumann boundary data on $\Gamma_N:=\Gamma_{fN}\cup\Gamma_{sN}$ and are combined to g . Analogously, the Dirichlet boundary data v_f^D and v_s^D on parts of $\partial\Omega$ are merged into a suitable velocity field $v^D\in\mathcal{V}$. The right hand side functions f_f and f_s are combined to f . The Cauchy stress tensor is again defined areawise on the whole domain by

$$\sigma(x):=\begin{cases}\sigma_f(x), & x-u(x)\in\hat\Omega_f,\\ \sigma_s(x), & x-u(x)\in\hat\Omega_s\cup\hat\Gamma_i.\end{cases}$$

Analogously, we introduce the characteristic functions of the (unknown) subdomains Ω_f and Ω_s by

$$\chi_f(x) := \begin{cases} 1, & x - u(x) \in \hat{\Omega}_f, \\ 0, & x - u(x) \in \hat{\Omega}_s \cup \hat{\Gamma}_i, \end{cases} \quad , \quad \chi_s := 1 - \chi_f.$$

The above definitions imply that we need to provide some kind of deformation u not only on the structure but also on the fluid domain. This is accomplished by the concept of the "Initial Position (IP) set" introduced below.

5.2.1 The IP set approach

We recall that for rewriting the structure equations in an Eulerian framework, we need the pressure $\hat{p}_s$, displacement $\hat{u}_s$, and its gradient $\hat{\nabla}\hat{u}_s$ expressed in the Eulerian sense, which are denoted by p_s, u_s, and ∇u_s, respectively. There holds

$$p_s(x) = \hat{p}_s(T(x)) = \hat{p}_s(\hat{x}), \quad u_s(x) = \hat{u}_s(T(x)) = \hat{u}_s(\hat{x}), \tag{5.6}$$

where T is the (inverse) displacement function of points in the deformed domain Ω_s back to points in the initial domain $\hat{\Omega}_s$,

$$\begin{aligned} &\hat{T} : \hat{\Omega}_s \to \Omega_s, \quad \hat{T}(\hat{x}) = \hat{x} + \hat{u}_s = x, \\ &T : \Omega_s \to \hat{\Omega}_s, \quad T(x) = x - u_s = \hat{x}. \end{aligned} \tag{5.7}$$

Since $\det\hat{\nabla}\hat{T} = \det\hat{F} \neq 0$ the displacements T and $\hat{T}$ are well defined. Further, for the deformation gradient, we found the relation $\hat{\nabla}\hat{u} = (I - \nabla u)^{-1} - I$.

The immediate difficulty with the above relations is that u_s is only implicitly determined by $\hat{u}_s$, since $T(x)$ also depends on u_s. This is unpractical, and we therefore need a direct way of determining the displacement $u(x)$ of a "material" point located at x with respect to its initial position at point $\hat{x}$. To achieve this, we introduce the so-called *"set of initial positions"* (IP set) $\varphi(\Omega, t)$ of all points of Ω at time t. If we look at a given "material" point at the position $x \in \Omega$ and the time $t \in (0, T]$, then the value $\varphi(x, t)$ will tell us what the initial position of this point was at time $t = 0$. These points are transported in the full domain with a certain velocity w. The convection velocity in the structure will be the structure velocity itself, $w_{|\Omega_s} = v_s$. If the fluid velocity were to be used for convection in the fluid domain, then the displacements there would eventually become very entangled. For this reason, we use an alternative velocity. With this notation, the mapping φ is determined by the following variational problem.

Problem 8 (Variational IP set problem)**.** *Find $\varphi(\cdot, t) \in \varphi_0 + V^0$, $t \in I$, such that*

$$(\partial_t\varphi + w \cdot \nabla\varphi, \psi) = 0 \quad \forall\psi \in V^0. \tag{5.8}$$

where φ_0 is a suitable extension of the Dirichlet data along the boundaries,

$$\begin{aligned} &\varphi(x, 0) = x, \quad x \in \Omega, \\ &\varphi(x, t) = x, \quad \{x, t\} \in \partial\Omega \times (0, T]. \end{aligned}$$

This means that $\hat{x} + \hat{u}(\hat{x}, t) = x$, for any point with the initial position $\hat{x}$ and the position x later at time t. Since $\hat{x} = \varphi(\hat{x}, 0) = \varphi(x, t)$ and $\hat{u}(\hat{x}, t) = u(x, t)$ it follows that

$$x = \varphi(x, t) + u(x, t). \tag{5.9}$$

Using this in the IP set equation (5.8) yields

$$(\partial_t u - w + w \cdot \nabla u, \psi) = 0 \quad \forall \psi \in V^0. \tag{5.10}$$

The interface Γ_i will usually intersect mesh cells. Due to this, we need a reasonable continuation of the displacement and its gradient from the structure domain into the fluid domain. The value of u in the fluid domain will be determined by the choice of the convection velocity w. If we were to use the fluid velocity this would eventually lead to increasing entanglement, which would necessitate a continual reinitialization of the IP set. As an alternative, we use the harmonic continuation of the structure velocity v_s to the whole domain Ω, which is likewise denoted by w and satisfies

$$(\chi_s(w - v), \psi) + \alpha_w \big\{ (\chi_f \nabla w, \nabla \psi) - (\partial_n w, \psi)_{\Gamma_i} \big\} = 0, \quad \forall \psi \in V^0, \tag{5.11}$$

where α_w is a small positive parameter. However, any other continuous extension of v_s satisfying physically reasonable boundary conditions would serve the same purpose. By this construction, the deflection u_f in the fluid domain becomes an artificial quantity without any real physical meaning, i.e., $d_t u_s = v_s$, but generally $d_t u_f \neq v_f$.

5.2.2 Eulerian formulation of the FSI problem:

Now, we can combine the Eulerian formulations of the flow and the structure part of the problem into a complete variational formulation of the nonstationary as well as the stationary FSI problem in Eulerian framework. In the case of STVK material the (non-physical) pressure p_s in the structure subdomain is determined as harmonic extension of the flow pressure p_f.

Problem 9 (Eulerian formulation of FSI problem)**.** *Find fields* $\{v, p, w, u\} \in \{v^D + \mathcal{V}^0\} \times \mathcal{L} \times \mathcal{V}^0 \times \mathcal{V}^0$, *such that* $v(0) = v^0$, $u(0) = u^0$, *and*

$$\begin{aligned}
(\rho(\partial_t v + v \cdot \nabla v), \psi) + (\sigma, \varepsilon(\psi)) &= (g_3, \psi)_{\partial\Omega} + (f_3, \psi), \\
(\mathrm{div} v, \chi) &= 0 \quad \textit{(INH)}, \\
(\chi_f \mathrm{div} v, \chi) + \alpha_p \big\{ (\chi_s \nabla p, \nabla \chi) - (\partial_n p, \chi)_{\Gamma_i} \big\} &= 0 \quad \textit{(STVK)}, \\
(\partial_t u - w + w \cdot \nabla u, \xi) &= 0, \\
(\chi_s(w - v), \varphi) + \alpha_w \big\{ (\chi_f \nabla w, \nabla \varphi) - (\partial_n w, \varphi)_{\Gamma_i} \big\} &= 0,
\end{aligned} \tag{5.12}$$

for all $\{\psi, \chi, \xi, \varphi\} \in V^0 \times L \times V^0 \times V^0$, *where* α_p, α_w *are small positive constants,* $F := (I - \nabla u)^{-1}$, $J := \det F$, $E := \frac{1}{2}(F^T F - I)$,

$$\chi_f := \begin{cases} 1, & x - u \in \hat{\Omega}_f \setminus \hat{\Gamma}_i, \\ 0, & x - u \in \hat{\Omega}_s, \end{cases} \qquad \chi_s = 1 - \chi_f,$$

and

$$\sigma|_{\Omega_f} := -pI + 2\rho_f\nu_f\varepsilon(v),$$
$$\sigma|_{\Omega_s} := \begin{cases} -pI + \mu_s(FF^T - I) & \textit{(INH)}, \\ J^{-1}F(\lambda_s(\mathrm{tr}E)I + 2\mu_s E)F^T & \textit{(STVK)}. \end{cases}$$

In this variational formulation the position of the fluid structure interface Γ_i is implicitly given by the displacement u and the characteristic function χ_s,

$$\Gamma_i(t) = \{x \in \Omega,\ x - u(x,t) \in \hat{\Gamma}_i\}. \tag{5.13}$$

Notice that the system (5.12) is *nonlinear* even if the two subproblems are linear, e.g., for a Stokes fluid interacting with a linear elastic structure.

In some situations the solution of an FSI problem may tend to a "steady state" as $t \to \infty$. For later purposes, we derive the set of equations determining such a steady state solution $\{v^*, p^*, w^*, u^*\} \in \{v^D + V^0\} \times L \times V^0 \times V^0$. The corresponding limits of the characteristic functions and subdomains are denoted by χ_f^*, χ_s^* and Ω_f^*, Ω_s^*, respectively. Further, the fluid velocity becomes constant in time, $v_f^* := \lim_{t\to\infty} v|_{\Omega_f}$, and the structure velocity vanishes, $v_s^* \equiv 0$, which in turn implies $w^* \equiv 0$. The steady state structure displacement u_s^* is likewise well defined, but the corresponding ("non-physical") fluid displacement is merely defined by $u_f^* = u_f^{\lim} := \lim_{t\to\infty} u|_{\Omega_f}$ and therefore depends on the chosen construction of $w|_{\Omega_f}$ as continuation of $w|_{\Omega_s}$. Actually, it could be defined by any suitable continuation of u_s^* to all of Ω, e.g., by harmonic continuation. On the other hand the steady state pressure p^* is to be determined from the limiting equations. Then, with suitable extensions u^D and v^D of the prescribed Dirichlet data on $\partial\Omega$, the FSI system (5.12) reduces to the following "stationary" form (for simplicity dropping the stars):

Problem 10 (Eulerian formulation of stationary FSI problem)**.** *Find* $\{v, p, u\} \in \{v^D + V^0\} \times L \times \{u^D + V^0\}$, *such that*

$$\begin{aligned} (\rho v \cdot \nabla v, \psi) + (\sigma, \varepsilon(\psi)) &= (g_3, \psi)_{\partial\Omega} + (f_3, \psi), \\ (\mathrm{div} v, \chi) &= 0 \quad \textit{(INH)}, \\ (\chi_f \mathrm{div} v, \chi) + \alpha_p\big\{(\chi_s \nabla p, \nabla\chi) - (\partial_n p, \chi)_{\Gamma_i}\big\} &= 0 \quad \textit{(STVK)}, \\ (\chi_f(u - u_f^{\lim}), \varphi) + (\chi_s v, \varphi) &= 0, \end{aligned} \tag{5.14}$$

for all $\{\psi, \chi, \varphi\} \in V^0 \times L \times V^0$, *where* $F := (I - \nabla u)^{-1}$, $J := \det F$, $E := \frac{1}{2}(F^T F - I)$, *and*

$$\sigma|_{\Omega_f} := -pI + 2\rho_f\nu_f\varepsilon(v),$$
$$\sigma|_{\Omega_s} := \begin{cases} -pI + \mu_s(FF^T - I) & \textit{(INH)}, \\ J^{-1}F(\lambda_s(\mathrm{tr}E)I + 2\mu_s E)F^T & \textit{(STVK)}. \end{cases}$$

In the following Table 1, we summarize the two monolithical variational formulations of the FSI problem, the (arbitrary) Lagrangian-Eulerian (ALE) and the (fully) Eulerian formulation.

Table 1: *Overview of variational formulations of the FSI problem for INH material: ALE (left) and Eulerian (right)*

I) ALE formulation	*II) Eulerian formulation*
$\hat{\Omega} = \hat{\Omega}_f \cup \hat{\Gamma}_i \cup \hat{\Omega}_s$	$\Omega = \Omega_f \cup \Gamma_i \cup \Omega_s$
Find $\{\hat{v}, \hat{p}, \hat{u}\}$ *for* $\hat{v}(0)$, $\hat{u}(0)$ *with*	*Find* $\{v, p, w, u\}$ *for* $v(0)$, $u(0)$ *with*
$(\rho\hat{J}\partial_t\hat{v} + \hat{\chi}_f\rho\hat{J}(\partial_t\hat{u} - \hat{v}) \cdot \widehat{\nabla}\hat{v}\hat{F}^{-1}, \hat{\psi})$ $+ (\hat{J}\hat{\sigma}\hat{F}^{-T}, \hat{\varepsilon}(\hat{\psi})) = \hat{f}(\hat{\psi})$	$(\rho\partial_t v + \rho v \cdot \nabla v, \psi) + (\sigma, \varepsilon(\psi)) = f(\psi)$
$(\hat{\chi}_s(\hat{J}-1) + \hat{\chi}_f\widehat{\mathrm{div}}(\hat{J}\hat{v} \cdot \hat{F}^{-T}), \hat{\chi}) = 0$	$(\mathrm{div} v, \chi) = 0$
$(\partial_t\hat{u} - \hat{\chi}_s\hat{v}, \hat{\varphi}) + \hat{\alpha}_u\big\{(\hat{\chi}_f\widehat{\nabla}\hat{u}, \widehat{\nabla}\hat{\varphi})$ $- (\hat{\partial}_n\hat{u}, \hat{\varphi}^u)_{\hat{\Gamma}_i}\big\} = 0$	$(\chi_s(w-v), \varphi) + \alpha_w\big\{(\chi_f\nabla w, \nabla\varphi)$ $- (\partial_n w, \varphi)_{\Gamma_i}\big\} = 0$
$(\partial_t u - w + w \cdot \nabla u, \xi) = 0$	
(*harmonically continued* $\hat{u}_s$ *into* Ω_f)	(*harmonically continued* w_s *into* Ω_f)
for all test fields $\{\hat{\psi}, \hat{\chi}, \hat{\varphi}\}$, *where*	*for all test fields* $\{\psi, \chi, \xi, \varphi\}$, *where*
$\hat{\chi}_s(\hat{x}) := \begin{cases} 0, & \hat{x} \in \hat{\Omega}_f \\ 1, & \hat{x} \in \hat{\Omega}_s \cup \hat{\Gamma}_i \end{cases}$	$\chi_s(x) := \begin{cases} 0, & x - u \in \hat{\Omega}_f \\ 1, & x - u \in \hat{\Omega}_s \cup \hat{\Gamma}_i \end{cases}$
$\hat{\chi}_f := 1 - \hat{\chi}_s$	$\chi_s := 1 - \chi_f$
$\hat{\sigma} := \begin{cases} -\hat{p}_f + \mu_f(\widehat{\nabla}\hat{v}_f\hat{F}^{-1} + \hat{F}^{-T}\widehat{\nabla}\hat{v}_f^T) \\ -\hat{p}_s + \mu_s(\hat{F}\hat{F}^T - I) \quad in\ \hat{\Omega}_s \cup \hat{\Gamma}_i \end{cases}$	$\sigma := \begin{cases} -p_f I + 2\mu_f\varepsilon(v_f) \quad in\ \Omega_f \\ -p_s I + \mu_s(FF^T - I) \quad in\ \Omega_s \end{cases}$
$\hat{F} := I + \widehat{\nabla}\hat{u}, \quad \hat{J} := \det\hat{F}$	$F := (I - \nabla u)^{-1}$

6 Discretization

In this section, we detail the discretization in space and time of the FSI problem based on its different variational formulations. Our method of choice is the Galerkin finite element (FE) method with "conforming" finite elements. For a general introduction to the FE method, we refer to Carey and Oden [15], Girault and Raviart [27], Brenner and Scott [12], and Braess [11]. First, we provide the framework for the finite element method. Then, we describe the complete variational formulations which are the basis of the Galerkin discretization. Since we are using a so-called "equal-order" approximation of all physical quantities, additional pressure stabilization has to be incorporated which is done here by the "local projection" technique of Becker and Braack [4]. The time discretization is by the first-order backward Euler scheme or the second-order Fractional-Step-θ scheme. We refer to Bristeau, Glowinski and Periaux [13], Rannacher [46, 47], and Glowinski [28] for a detailed discussion of these time discretization schemes.

At each time step a nonlinear algebraic problem is solved using a Newton-like

method. This relies on solving the linear defect-correction problem, which requires the evaluation of the corresponding Jacobi matrix. Due to the large size and the strongly nonlinear nature of the complete FSI problems in the ALE or the Eulerian frameworks, calculating the Jacobi matrix can be cumbersome. This difficulty is overcome following an approach that is also used in the method of "automatic differentiation", Griewank [29].

6.1 Mesh notation and finite element spaces

The spatial discretization is by a conforming finite element Galerkin method on meshes $\mathbb{T}_h$ consisting of cells denoted by K,

$$\bar{\Omega} = \bigcup_{i=1,..,N} \bar{K}_i \,,$$

which are (convex) quadrilaterals in 2d or hexahedrals in 3d. Such a decomposition $\mathbb{T}_h$ is referred to as "regular" if any cell edge is either a subset of the domain boundary components Γ_D, Γ_N, or a complete face or edge of another cell. However, to facilitate mesh refinement and coarsening, we allow the cells to have a certain number of nodes that are at the midpoint of sides or faces of neighboring cells. These "hanging nodes" do not carry degrees of freedom and the corresponding function values are determined by linear or bilinear interpolation of neighboring "regular" nodal points. For more details on this construction, we refer to Carey and Oden [15] or Bangerth and Rannacher [2].

The mesh parameter h is a scalar cellwise constant function defined by $h|_K := h_K = \mathrm{diam}(K)$. We set $h_{\max} := \max_{K\in\mathbb{T}_h} h_K$. For a cell K, we denote by ρ_K the diameter of the maximal inscribed ball of K and by $\alpha_K^{\max}$ its maximum interior angle. To ensure proper approximation properties of the finite element spaces which are constructed based on the meshes $\mathbb{T}_h$, we require the following regularity condition to be fulfilled:

Mesh regularity condition: *Each cell $K \in \mathbb{T}_h$ is the image of the reference unit cube $\hat{K} = [0,1]^d$ under some d-linear mapping $\sigma_K : \hat{K} \to K$. This mapping is uniquely described by the 2^d coordinate values of the corners of K, if the ordering of the corners is preserved, see Figure 3. The Jacobian tensors σ'_K of these mappings are invertible and satisfy the uniform bounds*

$$\sup_{h>0} \max_{K\in\mathbb{T}_h} \|\sigma'_K\| \le c, \qquad \sup_{h>0} \max_{K\in\mathbb{T}_h} \|(\sigma'_K)^{-1}\| \le c \tag{6.1}$$

This condition is satisfied if the cells $K \in \mathbb{T}_h$ possess the usual structural properties of uniform "non-degeneracy", "uniform shape", and "uniform size property".

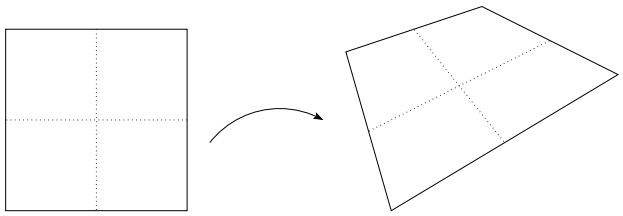

Figure 3: *Reference mapping* $\sigma_K : \hat{K} \to K$

To increase the number of cells in a decomposition $\mathbb{T}_h$, we employ "mesh refinement", which consists of subdividing a cell into 2^d subcells. Cell subdivision is done by connecting the midpoints of opposing edges or faces of a cell. A refinement is "global" if this is done for every cell. An example of a regular mesh and two global refinements is shown in Figure 4. Each of the resulting meshes after refinement is also regular. "Coarsening" of 2^d cells is possible if they were generated by prior refinement of some "parent cell". A group of 2^d such cells is referred to as a "(cell) patch".

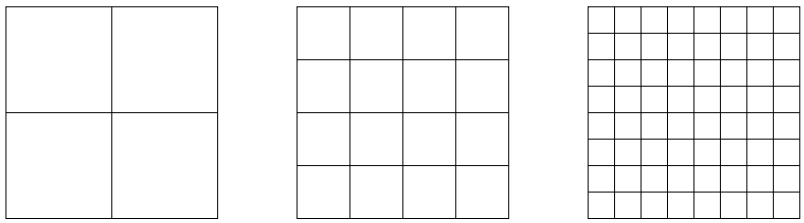

Figure 4: *A regular mesh after two cycles of global refinement*

In addition to "global" refinement, we will also use "local" refinement. This consists of only subdividing some cells in a given decomposition. Such refinement leads to cells nodes that are placed on the middle of the neighboring cells' edges or faces, i.e., to "hanging nodes", where only one hanging node is allowed per edge or face. In Figure 5 local refinement is applied twice leading to hanging nodes indicated by "dots".

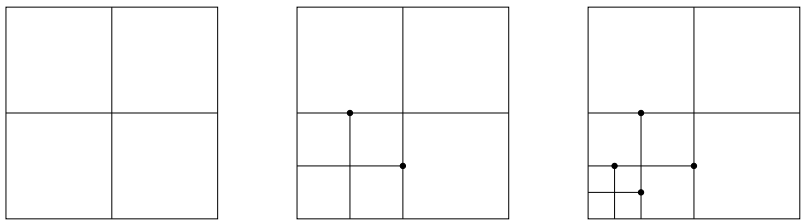

Figure 5: *A regular mesh after two cycles of local refinement*

Sometimes, we will require that a decomposition $\mathbb{T}_h$ is organized in a patch-wise manner. This means that $\mathbb{T}_h$ is the result of global refinement of the coarser decomposition $\mathbb{T}_{2h}$, as shown in Figure 6.

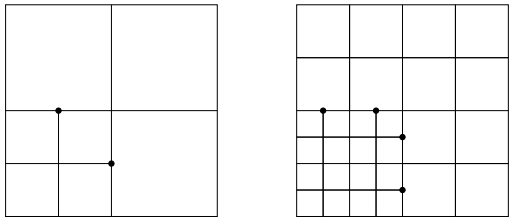

Figure 6: *A regular mesh after two cycles of patchwise local refinement*

Given a function space V the decomposition $\mathbb{T}_h$ and the cellwise space of polynomial functions $Q(K)$, we construct the corresponding finite element subspace $V_h \subset V$ by

$$V_h := \{\varphi \in V,\, \varphi|_K \in Q(K),\, K \in \mathbb{T}_h\}.$$

Each polynomial function space $Q(K)$ is actually defined on a "reference cell" $\hat{K} := (0,1)^d$ as the reference function space $\hat{Q}(\hat{K})$. The function space of polynomial degree $p \geq 0$ on $\hat{K}$ we denote as

$$\hat{Q}_p(\hat{K}) := \operatorname{span}\big\{\hat{x}^\alpha,\, \hat{x} = (\hat{x}_1, \ldots, \hat{x}_d) \in \hat{K},\, \alpha = (\alpha_1, \ldots, \alpha_d),\, \alpha_i \in \{0, \ldots, p\}\big\},$$

with the usual multi-index notation. In the numerical tests presented below, only finite elements with $p = 1$ ("d-linear elements") are used. Therefore, we omit the degree p and simply refer to $\hat{Q}(\hat{K})$. The reference function space $\hat{Q}(\hat{K})$ is mapped to the corresponding cell K with the help of the d-linear mapping $\sigma_K : \hat{K} \to K$,

$$Q(K) = \big\{\varphi(x) = \hat{\varphi}(\sigma_K^{-1}(x)),\, \hat{\varphi} \in \hat{Q}(\hat{K}),\, x \in K\big\}.$$

Since, in this case, the reference function space and the mapping function space are the same, the resulting finite elements are referred to as "isoparametric".

6.2 Galerkin formulation

For the discretization of Problems 6 and 7 (ALE framework) or 9 and 10 (Eulerian framework) in space, we use equal-order Q_1 finite elements as described above for all unknowns where the corresponding finite element subspaces are denoted by

$$L_h \subset L, \quad V_h \subset V, \quad W_h \subset W := V \times V \times V \times V.$$

Within the present abstract setting the discretization in time is likewise thought as by a Galerkin method, such as the dG(r) ("discontinuous" Galerkin) or cG(r) ("continuous" Galerkin) method of degree $r \geq 0$. The dG(0) method is closely related to the first-order backward Euler scheme (indeed even identical to this method for autonomous problems) and the cG(1) method to the second-order Crank-Nicolson scheme. However, in the test computations described below, we have used the Galerkin method only in space but the finite difference schemes in time. The full space-time Galerkin framework is mainly introduced as basis for a systematic approach to residual-based a posteriori error estimation as described below. In the following, we write the discretization only for the FSI problem written in the Eulerian framework. In the ALE framework it looks quite similar.

At first, we introduce a compact form of the variational formulation of the FSI problem. For arguments $U = \{v, p, w, u\}$ and $\Psi = \{\psi^v, \psi^p, \psi^w, \psi^u\} \in \mathcal{W} := \mathcal{V} \times \mathcal{V} \times \mathcal{V} \times \mathcal{V}$, we introduce the space-time semilinear form

$$\begin{aligned} A(U)(\Psi) \;:=\; \int_0^T \Big\{ & (\rho(\partial_t v + v \cdot \nabla v), \psi^v) + (\sigma(U), \varepsilon(\psi^v)) \\ & + \begin{cases} (\mathrm{div} v, \psi^p) & \text{(INH)} \\ (\chi_f \mathrm{div} v, \psi^p) + \alpha_p \big\{ (\chi_s \nabla p, \nabla \psi^p) - (\partial_n p, \psi^p)_{\Gamma_i} \big\} & \text{(STVK)} \end{cases} \\ & - (g_3, \psi^v)_{\partial\Omega} - (f_3, \psi^v) + (\partial_t u - w + w \cdot \nabla u, \psi^u) \\ & + (\chi_s(w - v), \psi^w) + \alpha_w \big\{ (\chi_f \nabla w, \nabla \psi^w) - (\partial_n w, \psi^w)_{\Gamma_i} \big\} \Big\}\, dt. \end{aligned}$$

With this notation, we can write the variational problem (9) in compact form.

Problem 11 (Compact Eulerian formulation of FSI problem)**.** *Find* $U \in U^D + \mathcal{W}^0$, *such that*

$$A(U)(\Psi) = 0 \quad \forall \Psi \in \mathcal{W}^0, \tag{6.2}$$

where U^D *is an appropriate extension of the Dirichlet boundary and initial data and the space* $\mathcal{W}^0$ *is defined by*

$$\mathcal{W}^0 := \big\{ \Psi = \{\psi^v, \psi^p, \psi^w, \psi^u\} \in \mathcal{V}^0 \times \mathcal{V}^0 \times \mathcal{V}^0 \times \mathcal{V}^0,\ \psi^u(0) = \psi^v(0) = 0 \big\}.$$

The spatial discretization by "equal-order" finite elements for velocity and pressure needs stabilization in order to compensate for the missing "inf-sup stability". We use the so-called *"local projection stabilization"* (LPS) introduced by Becker and Braack [4, 5]. An analogous approach is also employed for stabilizing the convection in the flow model as well as in the transport equation for the displacement u. Alternative methods of stabilization within Galerkin schemes us based the "upwind/Petrov-Galerkin" approach of Hughes, Brooks [36] and Hughes, Franca, Balestra [37].

We define the mesh-dependent bilinear form

$$(\varphi, \psi)_\delta := \sum_{K \in \mathbb{T}_h} \delta_K \, (\varphi, \psi)_K,$$

where the parameter δ_K is adaptively determined by

$$\delta_K := \frac{\alpha h_K^2}{\chi_f \rho_f \nu_f + \chi_s \mu_s + \beta \rho |v_h|_{\infty;K} h_K + \gamma |w_h|_{\infty;K} h_K}.$$

Further, we introduce the "fluctuation operator" $\pi_h : V_h \to V_{2h}$ on the finest mesh level $\mathbb{T}_h$ by $\pi_h := I - P_{2h}$, where $P_{2h} : V_h \to V_{2h}$ denotes the L^2-projection. The operator π_h measures the fluctuation of a function in V_h with respect to its projection into the next coarser space V_{2h}. With this notation, we define the stabilization form

$$\begin{aligned} S_\delta(U_h)(\Psi_h) \;:=\; \int_0^T \big\{ & (\nabla \pi_h p_h, \nabla \pi_h \psi_h^p)_\delta + (\rho v_h \cdot \nabla \pi_h v_h, v_h \cdot \nabla \pi_h \psi_h^v)_\delta \\ & + (w_h \cdot \nabla \pi_h u_h, w_h \cdot \nabla \pi_h \psi_h^u)_\delta \big\}\, dt, \end{aligned}$$

where the first term stabilizes the fluid pressure, the second one the INH structure pressure, the third one the transport in the flow model, and the fourth one the transport of the displacement u_h. The LP stabilization has the important property that it acts only on the diagonal terms of the coupled system and that it does not contain any second-order derivatives. However, it is only "weakly" consistent, as it does not vanish for the continuous solution, but it tends to zero with the right order as $h \to 0$. The choice of the numbers α, β, γ in the stabilization parameter δ_K is, based on practical experience, in our computations $\alpha = 1/2$, and $\beta = \gamma = 1/6$.

With this notation the stabilized Galerkin finite element approximation of problem (6.2) reads as follows.

Problem 12 (Spatial Galerkin approximation of FSI problem in Eulerian framework)**.** *Find* $U_h \in U_h^D + \mathcal{W}_h^0$*, such that*

$$A_\delta(U_h)(\Psi_h) := A(U_h, \Psi_h) + S_\delta(U_h)(\Psi_h) = 0 \quad \forall \Psi_h \in \mathcal{W}_h^0, \tag{6.3}$$

where the "discrete" finite element space $\mathcal{W}_h^0$ *is defined analogously as its "continuous" counterpart* $\mathcal{W}^0$*.*

As on the spatially continuous level the existence of solutions to this semi-discrete problem is not guaranteed and has to be justified separately for each particular situation.

6.3 Time discretization

The discretization in time is by the so-called *"Fractional-Step-θ scheme"* in which each time step $t_{n-1} \to t_n$ is split into three substeps $t_{n-1} \to t_{n-1+\theta} \to t_{n-\theta} \to t_n$. For brevity, we formulate this time stepping method for an abstract differential-algebraic equation (DAE) of the form

$$\begin{bmatrix} M & 0 \\ 0 & 0 \end{bmatrix} \begin{bmatrix} \dot{v}(t) \\ \dot{p}(t) \end{bmatrix} + \begin{bmatrix} A(v(t)) & B \\ -B^T & C \end{bmatrix} \begin{bmatrix} v(t) \\ p(t) \end{bmatrix} = \begin{bmatrix} b(t) \\ c(t) \end{bmatrix}, \tag{6.4}$$

which resembles the operator form of the spatially discretized incompressible Navier-Stokes equations with pressure stabilization. With the parameters $\theta = 1 - \sqrt{2}/2 = 0.292893...$, $\theta' = 1 - 2\theta$, $\alpha \in (1/2, 1]$, and $\beta = 1 - \alpha$, the fractional-step-θ scheme reads:

$$\begin{bmatrix} M + \alpha\theta k A^{n-1+\theta} & \theta k B \\ -B^T & C \end{bmatrix} \begin{bmatrix} v^{n-1+\theta} \\ p^{n-1+\theta} \end{bmatrix} = \begin{bmatrix} [M - \beta\theta k A^{n-1}]v^{n-1} + \theta k b^{n-1} \\ c^{n-1+\theta} \end{bmatrix}$$

$$\begin{bmatrix} M + \beta\theta' k A^{n-\theta} & \theta' k B \\ -B^T & C \end{bmatrix} \begin{bmatrix} v^{n-\theta} \\ p^{n-\theta} \end{bmatrix} = \begin{bmatrix} [M - \alpha\theta' k A^{n-1+\theta}]v^{n-1+\theta} + \theta' k b^{n-\theta} \\ c^{n-\theta} \end{bmatrix}$$

$$\begin{bmatrix} M + \alpha\theta k A^{n} & \theta k B \\ -B^T & C \end{bmatrix} \begin{bmatrix} v^{n} \\ p^{n} \end{bmatrix} = \begin{bmatrix} [M - \beta\theta k A^{n-\theta}]v^{n-\theta} + \theta k b_h^{n-\theta} \\ c^{n} \end{bmatrix},$$

where $A^{n-1+\theta} := A(x^{n-1+\theta})$, $b^{n-1} := b(t_{n-1})$, etc.. This scheme is of second order and has a similar work complexity as the well-known Crank–Nicolson scheme (case $\alpha = 1/2$). The fractional-step-θ scheme was originally proposed in form of

an operator splitting scheme separating the two complications "nonlinearity" and "incompressibility" within each cycle $t_{n-1} \to t_{n-1+\theta} \to t_{n-\theta} \to t_n$. However, it has also very attractive features as a pure time-stepping method. Being *strongly* A-stable, for any choice of $\alpha \in (1/2, 1]$, it possesses the full smoothing property in the case of rough initial data, in contrast to the Crank–Nicolson scheme which is only conditionally smoothing (for $k \sim h^2$). Furthermore, it is less dissipative than most of the other second-order implicit schemes and therefore suitable for computing oscillatory solutions; for more details, we refer to Bristeau, Glowinski and Periaux [13], Rannacher [46, 47], and Glowinski [28].

For computing steady state solutions, we use a pseudo-time stepping techniques based on the simple (first-order) backward Euler scheme, which in the notation from before reads

$$\begin{bmatrix} M+kA^n & kB \\ -B^T & C \end{bmatrix} \begin{bmatrix} v^n \\ p^n \end{bmatrix} = \begin{bmatrix} Mv^{n-1} + kb_h^{n-1} \\ c^n \end{bmatrix}.$$

6.4 Solution of the algebraic systems

After time and space discretization, in each substep of the fractional-step-θ scheme (or any other fully implicit time-stepping scheme) a quasi-stationary nonlinear algebraic system has to be solved. This is done by a standard Newton-type method with adaptive step-length selection, in which most of the nonlinear terms (i.e. the transport terms, the structure stress terms, the ALE mapping terms) are correctly linearized. Only the stabilization terms and the terms involving the characteristic function χ_f, determining the position of the interface, are treated by a simple functional iteration. In all cases the iteration starts from the values at the preceding time level. The resulting linear subproblems are then solved by the "Generalized Minimal Residual (GMRES)" method with preconditioning by a geometric multigrid method with block-ILU smoothing. Since such an approach is rather standard nowadays, we omit its details and refer to some relevant literature, e.g., Turek [54], Rannacher [46], or Hron and Turek [33]. For the implementational details of using the multigrid method on locally refined meshes, we refer to Becker and Braack [3].

6.5 Evaluation of directional derivatives

The resulting linear operator is essentially (if time-stepping parts and factors stemming from the approximation of the temporal derivatives are neglected) the directional derivatives of the governing semilinear form of the variational formulation, i.e. the form $A(U)(\Psi)$ in the Eulerian framework,

$$A'(U)(\Phi, \Psi) := \frac{d}{d\varepsilon} A(U + \varepsilon\Phi)(\Psi)|_{\varepsilon=0}. \tag{6.5}$$

For only "weakly nonlinear" systems such as the original Navier-Stokes equations in Eulerian framework obtaining the directional derivative is a straight forward task and can be done analytically "by hand". For structure mechanical systems (for example based on the St. Vernant-Kirchhoff material law) though writing down the explicit directional derivative can become a combersome. For example in the

Lagrangian case the scalar product $(\hat{J}\hat{F}^{-T}, \widehat{\nabla}\hat{\varphi}^v)$ is strongly nonlinear in $\hat{u}$,

$$\hat{J}\hat{\sigma}\hat{F}^{-T} = \hat{F}(\lambda_s \mathrm{tr}\hat{E}\, I + 2\mu_s \hat{E}), \quad \hat{F} = I + \widehat{\nabla}\hat{u}, \quad \hat{E} = \tfrac{1}{2}(\hat{F}^T\hat{F} - I).$$

However, in the Eulerian framework the corresponding scalar product takes the form $(\sigma, \nabla\varphi)$, which does not become any easier since the Cauchy stress tensor σ is based on the inverse of the "reverse deformation gradient" $I - \nabla u$,

$$\sigma = JF^{-1}(\lambda_s \mathrm{tr}E\, I + 2\mu_s E)F^{-T}, \quad F = I - \nabla u, \quad E = \tfrac{1}{2}(F^{-T}F^{-1} - I).$$

To alleviate this problem one may use a method that is the basis of "Automatic Differentiation" such as described in Rall [45] and Griewank [29]. The method is used to determine the derivative of a function at a given position. It is based on the technique of mechanically applying the basic rules of differentiation to the "serialized evaluation" of a function. This is achieved by breaking down the evaluation of the function for a given value into a sequence of basic elementary evaluations. Consequently, since evaluation is done in a sequence the resulting values from one evaluation are used in a later evaluation. To these elementary parts the rules of differentiation (i.e. the chain rule, the sum rule and the product rule) are applied.

The method of automatic differentiation lies between those of symbolic differentiation and the approximation of derivatives by divided differences. It is similar to symbolic differentiation in so far that the results are calculated by evaluating the same sequence of functions. It is thus just as accurate as symbolic differentiation. The difference is that, in contrast to symbolic differentiation, all "parsing" is done before compilation of the program, when the function evaluation is serialized and differentiation is applied to all levels of the serialization. This parsing before compilation is what gives the method a slight similarity to the method of divided differences. The full theory of automatic differentiation usually includes implementing the method in the form of a "precompiler" that completely relieves the user of applying the method and literally generates the derivatives in an automatic and efficient fashion. However, for the computational examples presented in this paper the method is used with differentiation done "by hand". In the first step, the "forward sweep", the function is broken down into a sequence of basic elementary evaluations. Each of these evaluations is stored in a variable. In the second step, the "reversed sweep", the rules of differentiation are applied. As a basic example, we present the calculation of the derivative of the function $f(x) := \sin(x\tanh(x))\log(x - 1/x)$ at the position x_0. The details of the realization of this method of automatic differentiation for the FSI problem formulated in the ALE or the Eulerian framework can be found in Dunne [22, 23].

Table 2: *Example of automatic differentiation*

forward sweep		reverse sweep
$f_1 := 1/x_0$		$f_1' := -1/x_0^2$
$f_2 := \log(x_0 - f_1)$		$f_2' := (1 - f_1')/(x_0 - f_1)$
$f_3 := \tanh(x_0)$	$\rightarrow$	$f_3' := 1 - \tanh^2(x_0)$
$f_4 := x_0 f_3$		$f_4' := f_3 + x_0 f_3'$
$f_5 := \sin(f_4)$		$f_5' := f_4' \cos(f_4)$
$f_6 := f_5 f_2$		$f_6' := f_5' f_2 + f_5 f_2'$
$f(x_0) := f_6$		$f'(x_0) := f_6'$

The only difference between the Eulerian and the ALE directional derivative are the differences of the directional derivatives concerning the displacement φ^u and $\hat{\varphi}^u$, respectively. In the Eulerian framework, we obtain "interface Dirac functions", whereas in the ALE framework the transformations acting on fluid equations are "derived". This problem is typically encountered in the field of shape optimization, see Sokolowski, Zolésio [50] and Allaire, de Gournay, Jouve, Toader [**?**]. For strong solutions $U = \{u, v, p\}$ and $\hat{U} = \{\hat{u}, \hat{v}, \hat{p}\}$, with $\hat{U}(\hat{x}) = U(\hat{x} + \hat{u}(\hat{x}))$ for $\hat{x} \in \hat{\Omega}$, of the different formulations of the FSI problem the directional derivatives with respect to velocity and pressure are equal. For the details, we again refer to Dunne [22, 23].

The directional derivatives play a direct role in the setup of the (linearized) "dual problem" which occurs in the method for a posteriori error estimation and "goal-oriented" mesh adaptation used in our test computations. The differences due to the use of the ALE or the Eulerian framework will be investigated at simple model situations, below.

7 Mesh adaptation

Now, we come to one of the main issues of this article, namely the automatic mesh adaptation within the finite element solution of the FSI problem. The computations shown in Sections 8 and 9, below, have been done on three different types of meshes:

- globally refined meshes obtained using several steps of uniform refinement of a coarse initial mesh,
- locally refined meshes obtained using a purely geometry-based criterion by marking all cells for refinement which have certain prescribed distances from the fluid-structure interface,
- locally refined meshes obtained using a systematic residual-based criteria by marking all cells for refinement which have error indicators above a certain threshold.

The ultimate goal is to employ the so-called *"Dual Weighted Residual Method"* (DWR method) for the adaptive solution of FSI problems. This method has been developed in Becker and Rannacher [7, 8] (see also Bangerth and Rannacher [2]) as an extension of the duality technique for a posteriori error estimation described in Eriksson, Estep, Hansbo, and Johnson [25]. The DWR method provides a general framework for the derivation of "goal-oriented" a posteriori error estimates together with criteria of mesh adaptation for the Galerkin discretization of general linear and nonlinear variational problems, including optimization problems. It is based on a complete *variational* formulation of the problem, such as (6.2) for the FSI problem. In fact, this was one of the driving factors for deriving the Eulerian formulation underlying (6.2). In order to incorporate also the time discretization into this framework, we have to use a fully space-time Galerkin method, i.e., a standard finite element method in space combined with the dG(r) or cG(r) ("discontinuous" Galerkin or "continuous" Galerkin) method in time. The following discussion assumes such a space-time Galerkin discretization, though in our test computations, we have used the fractional-step-θ scheme which is a difference scheme. Accordingly, in this paper the DWR method is used only in its stationary form in computing either steady states or intermediate quasi-steady states within the time stepping process.

7.1 The DWR method

We begin with the description of the DWR method for the special case of an FSI problem governed by an abstract variational equation such as (6.2). We restrict us to a simplified version of the DWR method, which suffices for the present purposes. For a more elaborated version, which is particularly useful in the context of optimization problems, we refer to the literature stated above. For notational simplicity, we think the nonhomogeneous boundary and initial data U^D to be incorporated into a linear forcing term $F(\cdot)$, or to be exactly representable in the approximating space $\mathcal{W}_h$. Then, we seek $U \in U^D + \mathcal{W}^0$ such that

$$A(U)(\Psi) = F(\Psi) \quad \forall \Psi \in \mathcal{W}^0. \tag{7.1}$$

The corresponding (stabilized) Galerkin approximation seeks $U_h \in U_h^D + \mathcal{W}_h^0$ such that

$$A(U_h)(\Psi_h) + S_\delta(U_h)(\Psi_h) = F(\Psi) \quad \forall \Psi_h \in \mathcal{W}_h^0. \tag{7.2}$$

Suppose that the goal of the computation is the evaluation of the value $J(U)$ for some functional $J(\cdot)$ (for simplicity assumed to be linear) which is defined on $\mathcal{W}$. We want to control the quality of the discretization in terms of the error

$$J(U - U_h) = J(U) - J(U_h).$$

To this end, we introduce the directional derivative $A'(U)(\Phi, \cdot)$ the existence of which is assumed. With the above notation, we introduce the bilinear form

$$L(U, U_h)(\Phi, \Psi) := \int_0^1 A'(U_h + s(U - U_h))(\Phi, \Psi)\, ds,$$

and formulate the "dual problem"

$$L(U,U_h)(\Phi,Z) = J(\Phi) \quad \forall \Phi \in \mathcal{W}^0. \tag{7.3}$$

In the present abstract setting the existence of a solution $Z \in \mathcal{W}^0$ of the dual problem (7.3) has to be assumed. Now, taking $\Phi = U - U_h \in \mathcal{W}^0$ in (7.3) and using the Galerkin orthogonality property

$$A(U)(\Psi_h) - A(U_h)(\Psi_h) = S_\delta(U_h)(\Psi_h), \quad \Psi \in \mathcal{W}_h^0,$$

yields the error representation

$$\begin{aligned} J(U-U_h) &= L(U,U_h)(U-U_h,Z) \\ &= \int_0^1 A'(U_h + s(U-U_h))(U-U_h,Z)\,ds \\ &= A(U)(Z) - A(U_h)(Z) \\ &= F(Z-\Psi_h) - A(U_h)(Z-\Psi_h) - S_\delta(U_h)(\Psi_h) \\ &=: \rho(U_h)(Z-\Psi_h) - S_\delta(U_h)(\Psi_h), \end{aligned}$$

where $\Psi_h \in \mathcal{W}^0$ is an arbitrary element, usually taken as the generic nodal interpolant $I_h Z \in \mathcal{W}_h^0$ of Z. For the evaluation of the terms on the right-hand side, we split the integrals in the residual term $\rho(U_h)(Z-\Psi_h)$ into their contributions from the single mesh cells $K \in \mathbb{T}_h$ and integrate by parts. This results in an estimate of the error $|J(U-U_h)|$ in terms of computable local residual terms $\rho_K(U_h)$ multiplied by certain weight factors $\omega_K(Z)$ which depend on the dual solution Z,

$$|J(U-U_h)| \le \sum_{K\in\mathbb{T}_h} \rho_K(U_h)\,\omega_K(Z) + |S_\delta(U_h)(\Psi_h)|. \tag{7.4}$$

The explicit form of the terms in the sum on the right-hand side will be stated for a special situation below. The second term due to the regularization is assumed to be small and is therefore neglected.

Since the dual solution Z is unknown, the evaluation of the weights $\omega_K(Z)$ requires further approximation. First, we linearize by assuming

$$L(U,U_h)(\Phi,\Psi) \approx L(U_h,U_h)(\Phi,\Psi) = A'(U_h)(\Phi,\Psi),$$

and use the approximate "discrete" dual solution $Z_h \in \mathcal{W}_h^0$ defined by

$$A'(U_h)(\Phi,Z_h) = J(\Phi_h) \quad \forall \Phi_h \in \mathcal{W}_h^0. \tag{7.5}$$

From Z_h, we generate improved approximations to Z in a post-processing step by patchwise higher-order interpolation. For example in 2d on 2×2-patches of cells in $\mathbb{T}_h$ the 9 nodal values of the piecewise bilinear Z_h are used to construct a patchwise biquadratic function $\tilde{Z}$ as indicated in Figure 7. This is then used to obtain the approximate error estimate

$$|J(U-U_h)| \approx \eta := \sum_{K\in\mathbb{T}_h} \rho_K(U_h)\,\omega_K(\tilde{Z}), \tag{7.6}$$

which is the basis of automatic mesh adaptation.

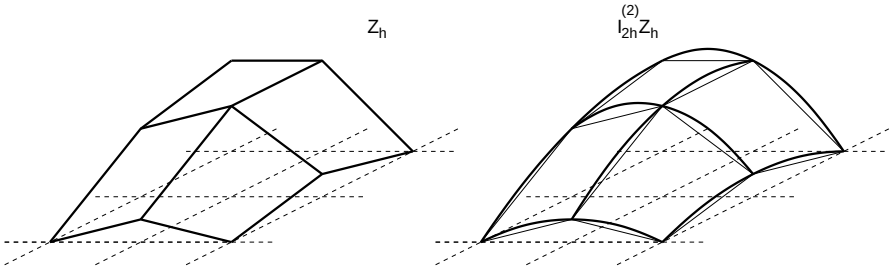

Figure 7: *Local postprocessing by patchwise "biquadratic" interpolation,* $I_{2h}^{(2)} Z_h$ *, of the "bilinear" discrete solution* Z_h *in 2D*

Remark 1. *The dual solution* Z *has the features of a "generalized" Green function* $G(K, K')$ *, as it describes the dependence of the target error quantity* $J(U - U_h)$ *, which may be concentrated at some cell* K *, on local properties of the data, i.e. in this case the residuals* $\rho_{K'}$ *on cells* K' *; see Figure 8.*

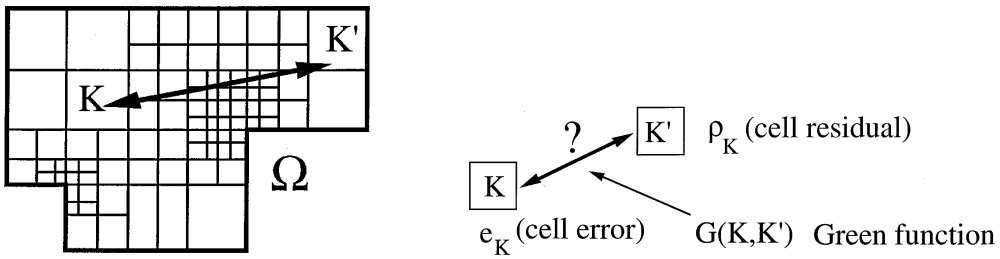

Figure 8: *Finite element mesh and scheme of error propagation*

Remark 2. *The solvability of the primal and dual problems (7.1), (7.2) and (7.3), (7.5), respectively, is not for granted. This is a difficult task in view of the rather few existence results in the literature for general FSI problems. Further, the assumption of differentiability cause concerns in treating the FSI problems in the Eulerian framework since the dependence of the characteristic function* $\chi_f(x - u)$ *on the deflection* u *is generally not differentiable (only Lipschitzian). However, this non-differentiability can be resolved by the "Hadamard structure theorem", on the assumption that the interface between fluid and structure forms a lower dimensional manifold and the differentiation is done in a weak variational sense. In essence this has the same effect as discretizing along the interface and replacing the directional derivative by a mesh-size dependent difference quotient, a pragmatic approach that has proven itself in similar situations, e.g. for Hencky elasto-plasticity in Rannacher and Suttmeier [48].*

For the *primal* problem the directional (Gâteaux) derivative of the complete FSI problem does not need to be exact, it only needs to be "good enough" for

Newton iteration to ensure convergence, leading to a reduction of the residuals of the nonlinear system. Thus, for the primal problem the nonlinear system is used to measure the "quality" of the approximation. For the *dual* problem though things may initially seem less clear, since the dual problem is simply a *linear* problem directly based on the Gâteaux derivative. Of course, an immediate "measure of quality" of the discrete dual solution is the residual of the linear system. But there is no immediate measure for the quality of the discrete dual solution in relation to the *continuous* dual solution. This uncertainty stems from the highly nonlinear influence of the displacement u in the Gâteaux derivative. For the ALE framework this is seen in the transformed fluid equations. For the Eulerian framework this is seen in additional boundary Dirac integrals, which stem from the shape derivatives. This seemingly lack of clarity though is not typical to FSI problems. It is only more obvious in such problems since everything *visible* depends on the position of the interface. Generally though this uncertainty concerning the discrete dual solution is present in *all* nonlinear problems, since in such problems the Gâteaux derivatives depend on the primal solution and can only be approximated by using the discrete primal solutions.

In the case of FSI problems, we assume that the interface obtained on the current mesh is already in good agreement with the correct one, $\Gamma_{hi} \approx \Gamma_i$, and set up the dual problem formally with Γ_{hi} as a fixed interface. This approach has proven very successful in similar situations, e.g., for Hencky elasto-plasticity in Rannacher and Suttmeier [48]. In all test computations, we did not encounter difficulties in obtaining the discrete solutions. In fact the performance of the error estimator for a given goal functional was always good for both the ALE and the Eulerian framework.

A common measure of the accuracy of the error estimator is the *"effectivity index"* defined by

$$I_{\text{eff}} := \frac{\eta}{|J(U-U_h)|},$$

which is the overestimation factor of the error estimator. It should desirably be close to one. A second quality measure for the error estimator is how effective its results are as indicators for adaptive mesh refinement. The error indicators $\eta_K := \rho_K \omega_K$ are the cellwise contributions of the error estimator

$$\eta = \sum_{K \in \mathbb{T}_h} \eta_K.$$

Again, in all our test computations the error estimator performed well for both the ALE and the Eulerian frameworks.

7.2 Mesh adaptation algorithm.

The approach we use for the adaptive refinement of the spatial mesh is straightforward. Particularly, for the refinement criteria there exist much more sophisticated versions, which are not used here for sake of simplicity. Let an error tolerance TOL be give. Then, on the basis of the (approximate) a posteriori error estimate (7.6), the mesh adaptation proceeds as follows:

1. Compute the primal solution U_h from (7.2) on the current mesh, starting from some initial state, e.g., that with zero deformation.

2. Compute the solution $\tilde{Z}_h$ of the approximate discrete dual problem (7.5).

3. Evaluate the cell-error indicators $\eta_K := \rho_K(U_h)\,\omega_K(\tilde{Z}_h)$.

4. If $\eta < TOL$ then accept U_h and evaluate $J(U_h)$, otherwise proceed to the next step.

5. Determine the 30% cells with largest and the 10% cells with smallest values of η_K. The cells of the first group are refined and those of the second group coarsened. Then, continue with Step 1. (Coarsening usually means canceling of an earlier refinement. Further refinement may be necessary to prevent the occurrence of too many hanging nodes. In two dimensions this strategy leads to about a doubling of the number of cells in each refinement cycle. By a similar strategy it can be achieved that the number of cells stays about constant during the adaptation process within a time stepping procedure.

Remark 3. *The error representation (7.4) has been derived assuming the error functional $J(\cdot)$ as linear. In many applications nonlinear, most often quadratic, error functionals occur. An example is the spatial L^2-norm error*

$$J(U_h) := \|(U - U_h)(T)\|,$$

at the end time T. For nonlinear (differentiable) error functionals the DWR approach can be extended to yield an error representation of the form (7.4); see Becker and Rannacher [8], Bangerth and Rannacher [2].

Remark 4. *The DWR method can also be applied to optimization problems of the form*

$$\min_{q\in Q} J(u,q)\,! \qquad a(u,q)(\psi) = f(\psi) \quad \forall \psi \in \mathcal{V}^0,$$

for instance in the context of an FSI setting. To this end we introduce the Lagrangian functional $\mathcal{L}(u,q,\lambda) := J(u,q) + f(\lambda) - a(u,q)(\lambda)$, with the adjoint variable $\lambda \in \mathcal{V}$. Its stationary points $\{u,q,\lambda\}$ are possible solutions of the optimization problem. These are determined by the nonlinear variational equation (so-called KKT system)

$$\mathcal{L}'(u,q,\lambda)(\varphi,\chi,\psi) = 0 \quad \forall \{\varphi,\chi,\psi\} \in \mathcal{V}^0 \times Q \times \mathcal{V}^0,$$

which has saddle-point character. For the solutions $\{u_h, q_h, \lambda_h\}$ of the corresponding finite element Galerkin approximation, there are residual-based error estimates available similar to (7.6); see Becker and Rannacher [8], Bangerth and Rannacher [2].

7.3 A stationary special case.

We will develop the explicit form of the error representation (7.4) and the approximate dual problem (7.5) for the *stationary* FSI model with an "incompressible neo-Hookean" (INH) solid. We assume the system as being driven only by Dirichlet boundary conditions, i.e., volume and surface forces are zero, $f_3 \equiv 0$ and $g_3 \equiv 0$.

Let $\{v, p, w, u\} \in \{v^D + V^0\} \times L \times V^0 \times V^0$ be a steady state solution of the corresponding FSI model (5.12) determined by the system (5.14). In order to simplify the formulation of the corresponding dual problem, we omit higher order terms, e.g., in the Cauchy stress tensor for the structure. Since there is no movement in the structure domain, the mass conservation condition $\mathrm{div} v_s = 0$ is not practical for the sensitivity analysis. For this reason the conservation condition in the structure domain will be $\det(I - \nabla u) = 1$, from which we again omit the higher order terms by approximating $\det(I - \nabla u) - 1 \approx \mathrm{div} u = 0$. Then, the variational formulation of the stationary FSI problem further reduces to

$$A(U)(\Psi) = F(\Psi) \quad \forall \Psi \in W^0, \tag{7.7}$$

with the (time-independent) semilinear form

$$\begin{aligned} A(U)(\Psi) \; &:= (\rho v \cdot \nabla v, \psi^v) + (\sigma(U), \varepsilon(\Psi)) + (\chi_f \mathrm{div} v + \chi_s \mathrm{div} u, \psi^p) \\ &\quad + (\chi_f u + \chi_s v, \psi^u), \end{aligned}$$

and the linear functional $F(\Psi) := (\chi_f u_f, \psi^u)$. Here, the stress-strain relation is given by

$$\sigma(U) = \begin{cases} -pI + 2\rho_f \nu_f \varepsilon(v), & \text{in } \Omega_f, \\ -pI + 2\mu_s \varepsilon(u), & \text{in } \Omega_s. \end{cases}$$

where the (small-strain) approximation $FF^T - I \approx 2\varepsilon(\psi^u)$ has been used.

Suppose now that the discretization error is to be controlled with respect to some linear functional on W of the form $J(\Phi) = j^v(\varphi^v) + j^p(\varphi^p) + j^u(\varphi^u)$. In order to correctly set up the corresponding dual problem, we would have to differentiate the semi-linear form $A(U)(\Psi)$ with respect to all components of U. However, this is not directly possible since the unknown position of the interface Γ_i depends on the displacement function u in a non-differentiable way. Because of this difficulty, we will adopt a more heuristic approach which is rather common in solving problems with free (only implicitly determined) boundaries. We assume that the interface obtained on the current mesh is already in good agreement with the correct one, $\Gamma_{ih} \approx \Gamma_i$, and set up the dual problem formally with Γ_{ih} as a fixed interface.

Adopting these simplifications and dropping all stabilization terms leads us to the following approximate dual problem, in which we seek $Z = \{z^v, z^p, z^u\} \in W^0$, such that

$$\tilde{A}'(U_h)(\Phi, Z) = J(\Phi) \quad \forall \Phi = \{\varphi^v, \varphi^p, \varphi^u\} \in W^0, \tag{7.8}$$

with the bilinear form

$$\begin{aligned} \tilde{A}'(U_h)(\Phi, Z) &= (\rho v_h \cdot \nabla \varphi^v, z^v) + (\rho \varphi^v \cdot \nabla v_h, z^v) + (\sigma'(U_h)\varepsilon(\Phi), \varepsilon(Z)) \\ &\quad + (\chi_f \mathrm{div} \varphi^v + \chi_s \mathrm{div} \varphi^u, z^p) + (\chi_f \varphi^u + \chi_s \varphi^v, z^u), \end{aligned}$$

where

$$\sigma'(U_h)\varepsilon(U) := \begin{cases} -pI + 2\rho_f \nu_f \varepsilon(v), & \text{in } \Omega_{f,h}, \\ -pI + 2\mu_s \varepsilon(u), & \text{in } \Omega_{s,h}. \end{cases}$$

Let Z be a solution of (7.8) and Z_h its finite element approximation. To evaluate the approximate error estimate

$$J(U-U_h) \approx F(Z-Z_h) - A(U_h)(Z-Z_h),$$

we introduce two modified submeshes

$$\mathbb{T}_{hs} := \{K \cap \Omega_{s,h},\, K \in \mathbb{T}_h\}, \quad \mathbb{T}_{hf} := \{K \cap \Omega_{f,h},\, K \in \mathbb{T}_h\},$$

and their union $\tilde{\mathbb{T}}_h := \mathbb{T}_{hs} \cup \mathbb{T}_{hf}$. The mesh $\tilde{\mathbb{T}}_h$ differs only from $\mathbb{T}_h$ in so far that the cells that contain the fluid-structure interface are subdivided into fluid domain part and structure domain part. Now, by cellwise integration by parts and rearranging boundary terms, we obtain

$$\begin{aligned} J(U-U_h) = \sum_{K\in\tilde{\mathbb{T}}_h} \Big\{ &(\mathrm{div}\sigma(U_h) - \rho v_h \cdot \nabla v_h, z^v - z_h^v)_K - (\tfrac{1}{2}[\sigma(U_h)\cdot n], z^v - z_h^v)_{\partial K} \\ &- (\chi_f \mathrm{div} v_h + \chi_s \mathrm{div} u_h, z^p - z_h^p)_K - (\chi_f(u_h - u_f) + \chi_s v_h, z^u - z_h^u)_K \Big\}, \end{aligned}$$

where $[\cdot]$ denotes the jump across intercell boundaries Γ. If Γ is part of the boundary $\partial\Omega$ the "jump" is assigned the value $[\sigma \cdot n] = 2\sigma \cdot n$. We note that in this error representation the "cell residuals" $\{\mathrm{div}\sigma(U_h) - \rho v_h \cdot \nabla v_h\}|_K$, $\{\chi_f \mathrm{div} v_h + \chi_s \mathrm{div} u_h\}|_K$, and $\{\chi_f(u_h - u_f) + \chi_s v_h\}|_K$ represent the degree of consistency of the approximate solution U_h, while the "edge term" $\frac{1}{2}[\sigma(U_h)\cdot n]$ measures its "discrete" smoothness. These residual terms are multiplied by the weights (sensitivity factors) $z^v - z_h^v$, $z^p - z_h^p$, and $z^u - z_h^u$, respectively. From this error representation, we can deduce the following approximate error estimate

$$|J(E)| \approx \sum_{K\in\tilde{\mathbb{T}}_h} \eta_K, \quad \eta_K := \sum_{i=1}^{4} \rho_K^{(i)} \omega_K^{(i)}, \tag{7.9}$$

with the residual terms and weights

$$\begin{aligned} \rho_K^{(1)} &:= \|\mathrm{div}\sigma(U_h) - \rho v_h \cdot \nabla v_h\|_K, \quad \omega_K^{(1)} := \|Z - Z_h\|_K, \\ \rho_K^{(2)} &:= \tfrac{1}{2} h_K^{-1/2} \|[\sigma(U_h)\cdot n]\|_{\partial K}, \quad \omega_K^{(2)} := h_K^{1/2} \|z^v - z_h^v\|_{\partial K}, \\ \rho_K^{(3)} &:= \|\chi_f \mathrm{div} v_h + \chi_s \mathrm{div} u_h\|_K, \quad \omega_K^{(3)} := \|z^p - z_h^p\|_K, \\ \rho_K^{(4)} &:= \|\chi_f(u_h - u_f) + \chi_s v_h\|_K, \quad \omega_K^{(4)} := \|z^u - z_h^u\|_K. \end{aligned}$$

The weights $\omega^{(i)}$ are approximated, for instance by post-processing the discrete dual solution Z_h as described above. Then, the cellwise error indicators η_K can be used for the mesh adaptation process.

7.4 Numerical integration along the interface

In the Eulerian framework, regardless of the refinement technique used, the interface line will be intersecting cells. In these interface cells equations change, e.g. the constitutive equations of the stress tensor. In the structure-structure interaction

examples below only the material parameter of the structure changes. In the fluid-structure examples the constitutive equation of the stress tensor changes entirely. The primal approach for coping with the error at the interface is to increase the refinement. This is either done by employing zonal refinement along the whole interface or using sensitivity analysis as a guide for local refinement.

Of course the first cause for an error at the interface cells is when the discrete variables do not approximate the continuous values well enough. This error can only be resolved by cell refinement. If the error at the interface cells is in large parts only caused by quadrature errors, then refinement along the interface solely on this basis is expensive, since this increases the number of unknowns in the complete system. Additionally, even if the discrete variables do approximate the continuous values well, the quadrature error will still occur, due to the change in the model. Consider for example in Problem 10 the incompressibility condition for the fluid:

$$0 = (\chi_f \mathrm{div} v_h, \psi_h^p) = \sum_{K \in \mathbb{T}_h} \int_K \chi_f \mathrm{div} v_h \psi_h^p \, dx. \tag{7.10}$$

Generally, we will be using Gauß quadrature. This quadrature though is only good for smooth functions. For cells that are either completely in the fluid domain or in the structure domain the use of the Gauß quadrature is appropriate. But for interface calls , i.e. cells which are cut by the interface, this will lead to the cell integrals being wrongly weighted. In the context of equation (7.10) it will lead to the incompressibility condition either having a strong and undesirable influence on the structure velocity or on the other hand being influenced by the structure velocity. To reduce this error, we use an adaptive quadrature. On cells that are not cut by the interface, we continue using the Gauß rule. On the cells containing the interface, we use a more appropriate summed quadrature rule, which is based on the simple midpoint rule. This strategy has a very good effect on the quality of the approximation, and particularly on the mass conservation. For more details, we refer to Dunne [22, 23].

An additional source of discontinuous behavior is the exact evaluation of the characteristic functions. This stems from the way the basis functions on the cells couple, which may lead to a sudden on- and off-switching of the coupling between the nodes of interface cells and their neighbors, which in turn leads to sudden discontinuous behavior of node values. To alleviate this problem, we regularize the characteristic functions χ_f and $\chi_s := 1 - \chi_f$ like

$$\chi_{fh} := \tfrac{1}{2}\big(1 + \tanh(\alpha_\chi \varphi(x))\big), \qquad \chi_{sh} := 1 - \chi_{fh},$$

with a smoothing parameter α_χ and the signed distance function $\varphi(x) := (\chi_f - \chi_s)\mathrm{dist}(x, \Gamma_i)$. The smoothing parameter is chosen accordingly to the local mesh size h. We only use φ as a parameter to the tanh function, thus it is only necessary that it roughly approximate the distance. In the examples presented below material deformations at the interface are regular enough to allow the Eulerian distance function φ to be approximated by the reference domain distance $\varphi(x) \approx \hat{\varphi}(x - u)$ with $\hat{\varphi}(\hat{x}) := (\hat{\chi}_f - \hat{\chi}_s)\mathrm{dist}(\hat{x}, \hat{\Gamma}_i)$. This approach has similarity to the Volume-of-Fluid method (Hirt and Nichols [32]), since both use a "fraction of equation" variable similar to our approximation of χ_f. For more details, we refer to Dunne [22, 23].

8 Numerical test 1: elastic flow cavity

For validating the numerical method based on the Eulerian framework, we use a simple stationary test example, the lid-driven cavity with an elastic bottom wall, as shown in Figure 9. For simplicity, for modeling the fluid the linear Stokes equations are used and the material of the bottom wall is assumed to be linear neo-Hookean and incompressible. The structure material is taken as very soft such that a visible deformation of the fluid-structure interface can be expected. Then, the other material parameters are chosen such that flow and solid deformation velocity are small enough to allow for a stationary solution of the coupled linear systems. This solution is computed by a pseudo-time stepping method employing the implicit Euler scheme. A steady state is reached once the kinetic energy of the structure is below a prescribed small tolerance, here $\|v_s\|^2 \leq 10^{-8}$.

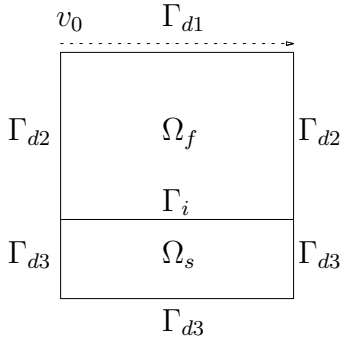

Figure 9: *Configuration of the "elastic" lid-driven cavity.*

The cavity has a size of 2×2, and its elastic part has a height of 0.5. The material constants are $\rho_f = \rho_s = 1$, $\nu_f = 0.2$, and $\mu_s = 2.0$. At the top boundary Γ_{d1} the regularized tangential flow profile

$$v_0 = 0.5 \begin{cases} 4x, & x \in [0.0, 0.25], \\ 1, & x \in (0.25, 1.75), \\ 4(2-x), & x \in [1.75, 2.0], \end{cases}$$

is prescribed, in order to avoid problems due to pressure singularities.

8.1 Computations on globally refined meshes

Figures 10 shows the final steady state computed on globally uniform meshes. In Figure 11, we monitor the development of $\|v_s\|^2$ during the pseudo-time stepping process depending on the number of cells of the mesh. As expected the kinetic energy tends to zero. The multiple "bumps" occur due to the way the elastic structure reaches its stationary state by "swinging" back and forth a few times. At the extreme point of each swing the kinetic energy has a local minimum. Figure 12 displays the mass error of the structure at the stationary state and find that it is actually of the expected order $O(h^2)$.

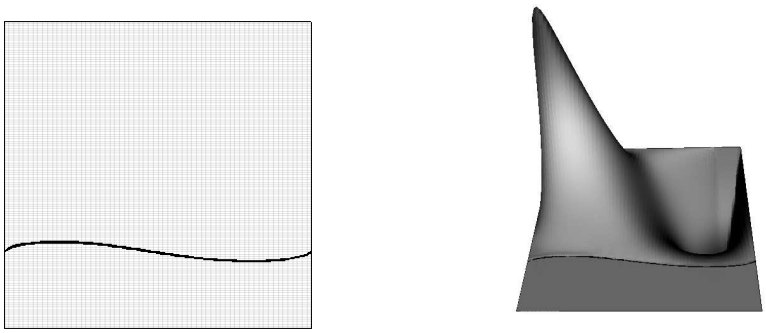

Figure 10: *Final position of interface (left) and vertical velocity (right)*

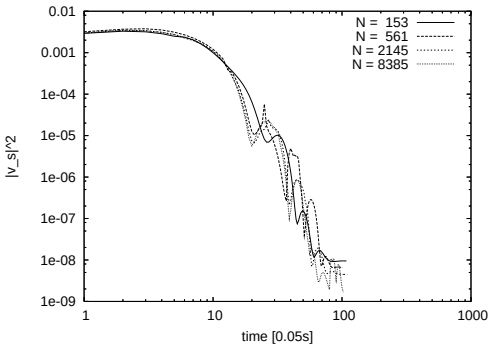

Figure 11: *Variation of $\|v_s\|^2$ in time for different numbers N of mesh cells.*

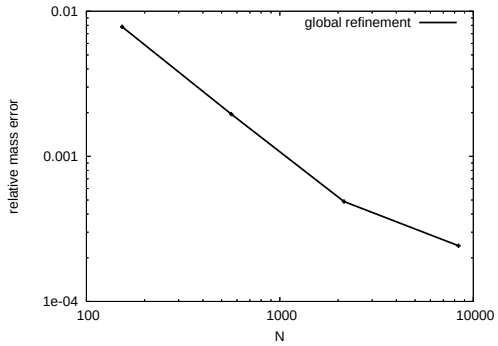

Figure 12: *Relative error of mass conservation in the steady state on globally and locally refined meshes.*

8.2 Computations on locally adapted meshes

Next, we apply the simplified stationary version of the DWR method as described in Section 7 for local mesh adaptation in the present test problem. For the "goal-oriented" a posteriori error estimation, we take the value of the pressure at the point $A = (0.5, 1.0)^T$ which is located in the flow region. To avoid sharp singularities in the corresponding dual solution, the associated functional is regularized to

$$J(u,p) = |K_A|^{-1} \int_{K_A} p\,dx \approx p(A),$$

where $K_A \in \mathbb{T}_h$ is a cell containing the point A. As reference value of $p(A)$, we use the result obtained on a very fine uniform mesh.

Figure 13 shows a sequence of adapted meshes. As expected two effects can be seen. There is local refinement around the point of interest and since the position of the fluid-structure interface is a decisive factor for the pressure field, local refinement also occurs along the interface.

In Figures 14 and 15 the resulting pressure error and the relative error in mass conservation is displayed as a function of the number of mesh cells.

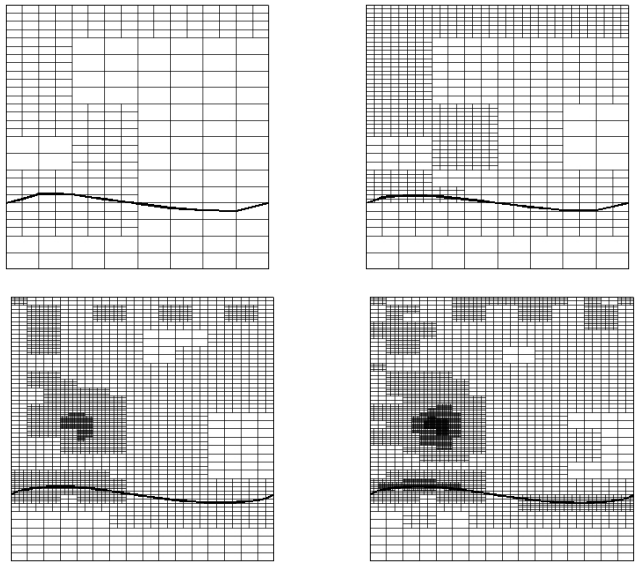

Figure 13: *Locally adapted meshes with* $N = 335, 1031, 3309, 5123$ *cells.*

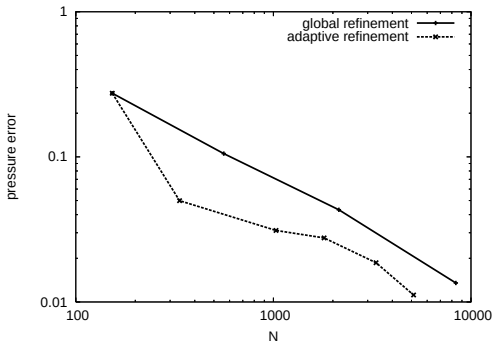

Figure 14: *Reduction of the pressure value error.*

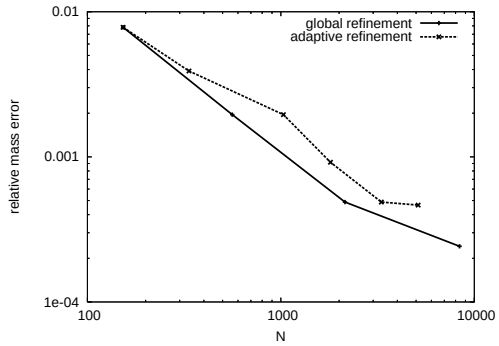

Figure 15: *Relative error of mass conservation.*

It may seem surprising that in Figure 15 there is no reduction of the mass error in the last iteration. This is due to the approach we are using here. After each step of mesh adaption a new primal solution is calculated, starting with the initial state of no deformation. The sensitivity analysis though does not take the initial state into account. Mesh adaption takes place around the final state of the interface, it does not reflect its initial state. An easy way of alleviating the mass error problem is to explicitly move a certain amount of local refinements with the interface from one time step to the next. Doing that though in this example would have made it unclear if the local refinement at the final interface position was due to the sensitivity analysis or the explicit movement of interface-bound refinement.

9 Numerical test 2: FSI benchmark FLUSTRUK-A

The second example is the FSI benchmark FLUSTRUK-A described in [34]. A thin elastic bar immersed in an incompressible fluid develops self-induced time-periodic oscillations of different amplitude depending on the material properties assumed. This benchmark has been defined to validate and compare the different computational approaches and software implementations for solving FSI problems. In order to have a fair comparison of our Eulerian-based method with the traditional Eulerian-Lagrangian approach, we have also implemented an ALE method for this benchmark problem. The configuration of this benchmark shown in Figure 16 is based on the well-known CFD benchmark "Flow Around a Cylinder", Turek and Schäfer [55].

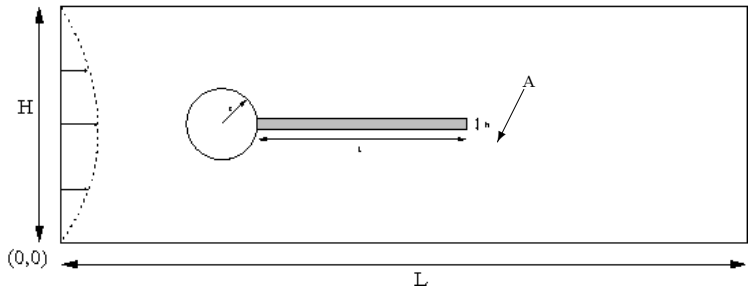

Figure 16: *Configuration of the FSI benchmark 'FLUSTRUK-A'.*

Configuration: The computational domain has length $L = 2.5$, height $H = 0.41$, and left bottom corner at $(0, 0)$. The center of the circle is positioned at $C = (0.2, 0.2)$ with radius $r = 0.05$. The elastic bar has length $l = 0.35$ and height $h = 0.02$. Its right lower end is positioned at $(0.6, 0.19)$ and its left end is clamped to the circle. Control points are $A(t)$ fixed at the trailing edge of the structure with $A(0) = (0.6, 0.20)$, and $B = (0.15, 0.2)$ fixed at the cylinder (stagnation point).

Boundary and initial conditions: The boundary conditions are as follows: Along the upper and lower boundary the usual "no-slip" condition is used for the velocity. At the (left) inlet a constant parabolic inflow profile,

$$v(0, y) = 1.5\,\bar{U}\,\frac{4y(H - y)}{H^2},$$

is prescribed which drives the flow, and at the (right) outlet zero-stress $\sigma \cdot n = 0$ is realized by using the "do-nothing" approach in the variational formulation, [31], [46]. This implicitly forces the pressure to have zero mean value at the outlet. The initial condition is zero flow velocity and structure displacement.

Material properties: The fluid is assumed as incompressible and Newtonian, the cylinder as fixed and rigid, and the structure as (compressible) St. Venant-Kirchhoff (STVK) type.

Discretization: The first set of computations is done on globally refined meshes for validating the proposed method and its software implementation. Then, for the same configuration adaptive meshes are used where the refinement criteria are either purely heuristic, i.e., based on the cell distance from the interface, or are based on a simplified stationary version of the DWR approach (at every tenth time step) as already used before for the cavity example. In all cases a uniform time-step size of $0.005\,s$ is used. The curved cylinder boundary is approximated to second order by polygonal mesh boundaries as can be seen in Figure 17.

The following four different test cases are considered:

- *Computational fluid dynamics test (CFD Test):* The structure is made very stiff, to the effect that we can compare the computed drag and lift coefficients with those obtained for a pure CFD test (with rigid structure).
- *Computational structure mechanics test (CSM Test):* The fluid is set to be initially in rest around the bar. The deformation of the bar under a vertical gravitational force is compared to the deformation of the same bar in a pure CSM test.
- *FSI tests:* Three configurations are treated corresponding to different inflow velocities and material stiffness parameters, and the Eulerian approach is compared to the standard ALE method.
- *FSI with large deflections:* The fluid is set to be initially in rest around the bar. The gravitational force on the bar is very large, causing a large deformation of the bar and eventually it reaching and running up against the channel wall. This case is difficult for the ALE method but can easily be handled by the Eulerian approach.

9.1 CFD test

Here, the structure is set to be very stiff to the effect that we can compare derived drag and lift values with those obtained with a pure CFD approach. The forces are calculated based on the closed path S around the whole structure, cylinder and bar,

$$J(u,p) := \int_S \sigma_f \cdot n \, do. \tag{9.1}$$

The CFD test has been done with the parameters listed in Table 3.

Parameters	CFD test
$\rho_f[10^3 kg\, m^{-3}]$	1
$\nu_f[10^{-3} m^2 s^{-1}]$	1
ν_s	0.4
$\rho_s[10^6 kg\, m^{-3}]$	1
$\mu_s[10^{12} kg\, m^{-1} s^{-2}]$	1
$U[m\, s^{-1}]$	1

Table 3: *Parameters for the CFD test.*

For the chosen parameters there is a steady state solution. The reference values for the drag and lift forces are calculated using a pure CFD approach on globally refined meshes (see also Hron and Turek [34]). The results are shown in Table 4. Using the Eulerian FSI approach, we calculate the same forces again. As a method of mesh adaption, we use a heuristic approach as described above.

N	dof	drag	lift	N	dof	drag	lift
1 278	3834	145.75	10.042	1 300	9100	122.66	12.68
4 892	14676	133.91	10.239	2 334	16338	126.13	11.71
19 128	57384	136.00	10.373	8 828	61796	132.17	11.93
75 632	226896	136.54	10.366	9 204	64428	131.77	10.53
300 768	902304	136.67	10.369	36 680	256760	134.47	10.45
∞	∞	136.70	10.530	∞	∞	136.70	10.530

Table 4: *CFD test: Results of CFD computation on uniform meshes (left), and by the Eulerian FSI approach on heuristically adapted meshes (right).*

9.2 CSM test

Here, the inflow velocity is set to be zero and the fluid is initially at rest. A vertical gravitational force is applied, which causes the bar to slowly sink in the fluid-filled volume. Due to the viscous effect of the fluid the bar will eventually come to rest. The value of final displacement can be compared to the results calculated with a pure CSM approach in a Lagrangian framework. The quantity of interest is the displacement of the point A at the middle of the trailing tip. The corresponding reference values are taken from [34]. The CSM test has been done with the parameters listed in Table 5. Using the Eulerian FSI approach, we calculate the displacements with mesh adaption by the heuristic approach described above. The final stationary positions and the heuristically adapted meshes can be seen in Figure 17.

parameter	CSM test
$\rho_f[10^3 kg\, m^{-3}]$	1
$\nu_f[10^{-3} m^2 s^{-1}]$	1
ν_s	0.4
$\rho_s[10^3 kg\, m^{-3}]$	1
$\mu_s[10^6 kg\, m^{-1} s^{-2}]$	0.5
$U[m\, s^{-1}]$	0
$g[m\, s^{-2}]$	2

Table 5: *Parameters for the CSM test.*

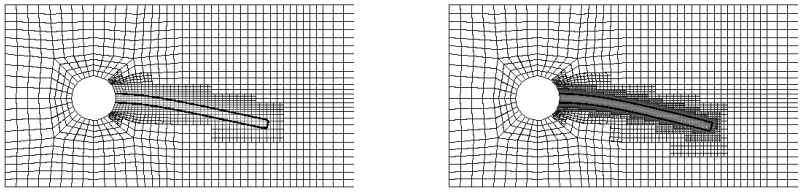

Figure 17: *CSM test: Stationary position of the control point A on heuristically refined meshes with $N = 1952$ and $N = 7604$ cells.*

N	dof	$u_x(A)$ $[10^{-3}m]$	$u_y(A)$ $[10^{-3}m]$
1952	13664	-5.57	-59.3
3672	25704	-6.53	-63.4
7604	53228	-6.74	-64.6
∞	∞	-7.187	-66.10

Table 6: *CSM test: Displacement of the control point A for three levels of heuristic mesh adaption.*

Next, we apply the DWR method as described above to the CSM test case. In the dual problem, we use the Jacobi matrix of the model as presented in Section 6. In the first example the DWR method was always applied to the final stationary state. The results were used for mesh adaption. The generated mesh was then used with the initially unperturbed problem to determine a new final stationary state. In contrast to that approach, we now apply the DWR method at periodic intervals without restarting. To control the resulting mesh adaption at each interval, we try to keep the number of nodes N below a certain threshold N_d. This is achieved by reducing refinement and/or increasing coarsening at each interval. As an example we calculate the point-value of the component sum of $u(A)$ at the control point A.

The position x_A is determined from $x_A - u(x_A) = A(0) = (0.6, 0.2)^T$. As a error control functional, we use a regularized delta function at x_A applied to $(e_1 + e_2)^T u$,

$$J(u) = |K_A|^{-1} \int_{K_A} (e_1 + e_2)^T u(x)\, dx \ ,$$

where K_A is the cell in the Mesh $\mathbb{T}_h$ containing the point A.

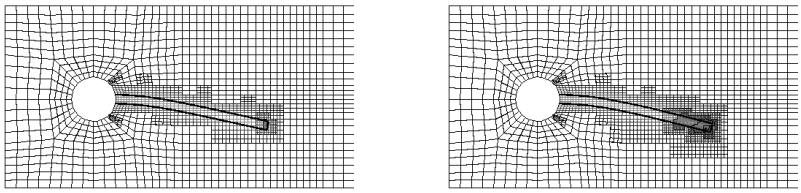

Figure 18: *CSM Test: Stationary position of the bar computed on locally refined meshes (DWR method) with* $N = 2016$ *and* $N = 4368$ *cells.*

N_d	N	dof	$u_x(A)$ $[10^{-3}m]$	$u_y(A)$ $[10^{-3}m]$
2000	2016	14112	-5.73	-59.8
3000	2614	18298	-6.54	-63.2
4500	4368	30576	-6.88	-64.6
	∞	∞	-7.187	-66.10

Table 7: *CSM Test: Displacements of the control point* A *for three levels of locally refined meshes (DWR method).*

9.3 FSI tests

Three test cases, FSI-2, FSI-3, and FSI-3*, are treated with different inflow velocities and material stiffness values as stated in Table 8. The parameters are chosen such that a visible transient behavior of the bar can be seen. The comparison values have been calculated using the ALE method on a very fine mesh. Using the Eulerian FSI approach, we calculate the displacements on three mesh levels, where the heuristic approach as described above is used for mesh refinement.

parameter	FSI-2	FSI-2*	FSI-3	FSI-3*
structure model	STVK	SZVK	STVK	INH
$\rho_f[10^3 kg\,m^{-3}]$	1	1	1	1
$\nu_f[10^{-3} m^2 s^{-1}]$	1	1	1	1
ν_s	0.4	0.4	0.4	0.5
$\rho_s[10^3 kg\,m^{-3}]$	10	20	1	1
$\mu_s[10^6 kg\,m^{-1} s^{-2}]$	0.5	0.5	2	2
$\bar{U}[m\,s^{-1}]$	1	0	2	2

Table 8: *Parameter settings for the FSI test cases.*

We begin with the FSI-2 and FSI-3 test cases. Some snapshots of the results of these simulations are shown in Figures 19 and 21. The time-dependent behavior of the displacements for the tests are shown in Figures 20 and 22. It can be seen that the time-periodic limit state is reached faster by the ALE method than by the Eulerian method. This phenomenon is observed also for the other test cases and therefore seems to be a characteristic feature of this particular version of the Eulerian method. In fact, we believe that it is the process of continuing the structure deformation into the fluid domain by harmonic extension (involving a sensible control parameter α_w), which causes the higher "stiffness" of the Eulerian model. However, this question needs further investigation.

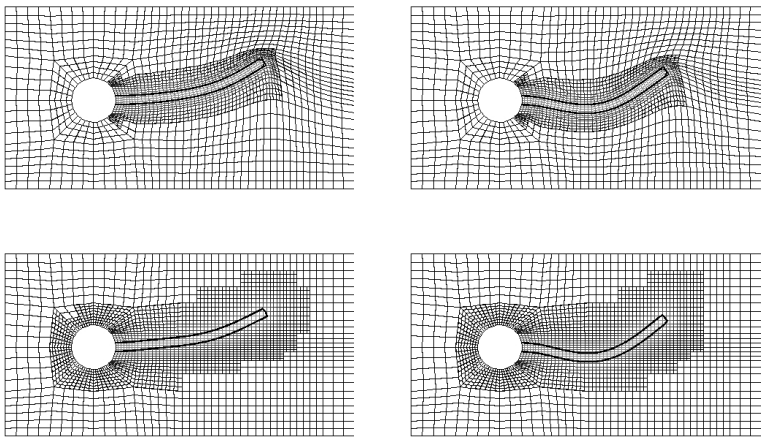

Figure 19: *FSI-2: Snapshots of results obtained by the ALE (top two) and by the Eulerian (bottom two) approaches.*

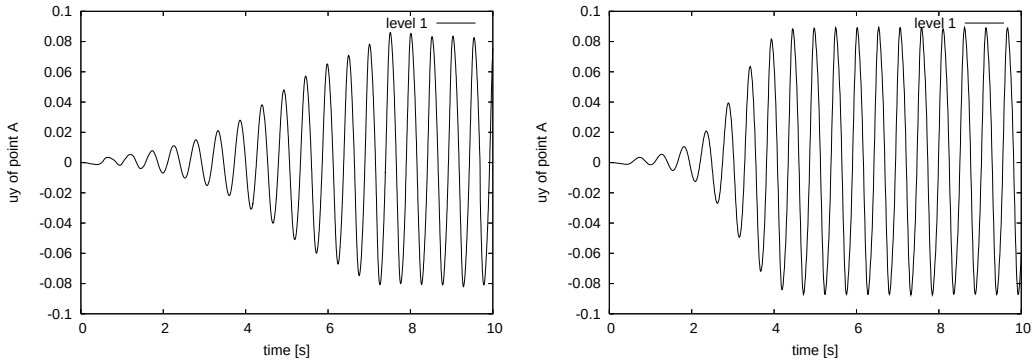

Figure 20: *FSI-2: Vertical displacement of the control point A, obtained by the Eulerian approach (left, $N = 2082$ cells) with max. amplitude $2.226 \cdot 10^{-2}$ and frequency $1.92\, s^{-1}$, and by the ALE approach (right, $N = 2784$ cells) with max. amplitude $2.68 \cdot 10^{-2}$ and frequency $1.953\, s^{-1}$.*

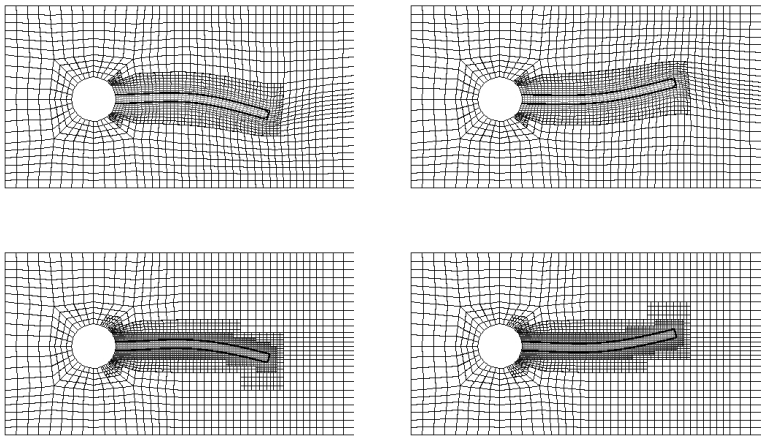

Figure 21: *FSI-3 Test: Some snapshots of results obtained by the ALE (top two) and the Eulerian (bottom two) approaches.*

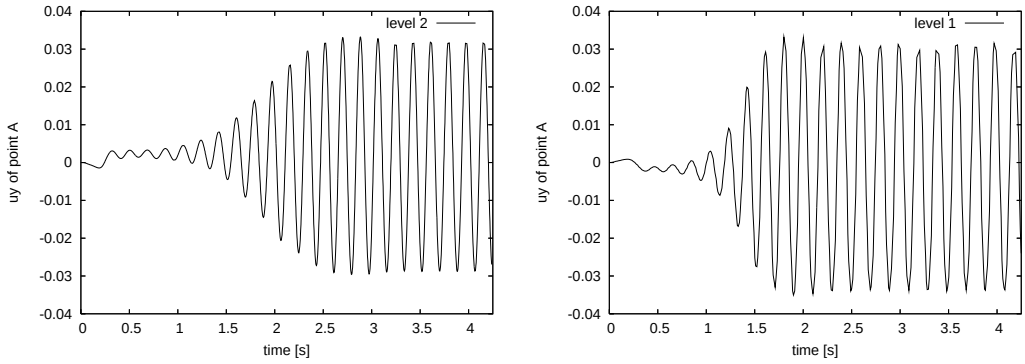

Figure 22: *FSI-3 Test: Vertical Displacement of the control point A, obtained by the Eulerian approach (left,* $N = 3876$ *cells) with max. amplitude* $6.01 \cdot 10^{-2}$ *and frequency* $5.48\,s^{-1}$*, and by the ALE approach (right,* $N = 2082$ *cells) with max. amplitude* $6.37 \cdot 10^{-2}$ *and frequency* $5.04\,s^{-1}$*.*

The FSI-3* test case is used to illustrate some special features of the Eulerian solution approach. Figure 23 illustrates the treatment of corners in the structure by the IP set approach compared to the LS approach. In the LS method the interface is identified by all points for which $\varphi = 0$, while in the IP set method the interface is identified by all points which are on one of the respective isoline segments belonging to the edges of the bar. The differences are visible in the cells that contain the corners.

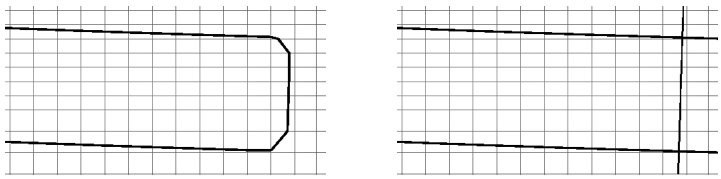

Figure 23: *FSI-3*: Treatment of corners by the LS method (left) and by the IP set method (right).*

Since in the Eulerian approach the structure deformations are not in a Lagrangian framework, it is not immediately clear, due to the coupling with the fluid, how well the mass of the structure is conserved in an Eulerian approach, especially in the course of an instationary simulation comprising hundreds of time steps. In Figure 24, we display the bar's relative mass error as a function of time. Except for certain initial jitters, the relative error is less than 1%.

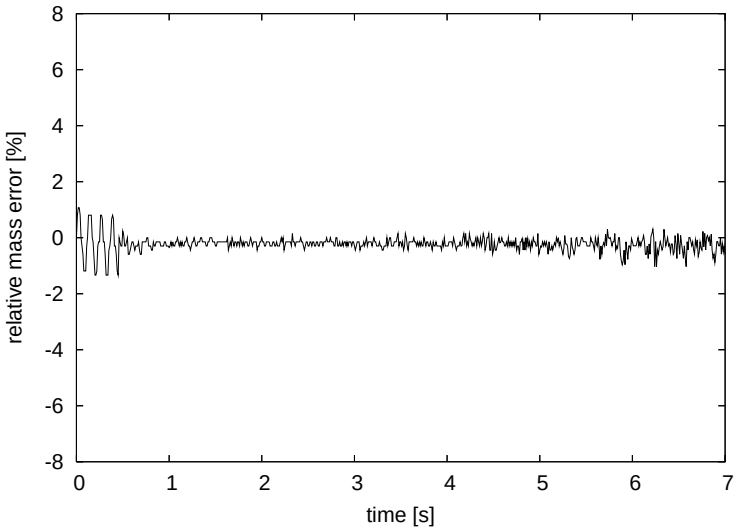

Figure 24: *FSI-3*: Relative mass error of the bar.*

Finally, Figure 25 illustrates the time dynamics of the structure and the adapted meshes over the time interval $[0, T]$. For both approaches, we obtain a periodic oscillation with maximum amplitudes and frequency, which are quite close to each other: 1.6e-2 versus 1.51e-2 and $6.86 s^{-1}$ versus $6.70 s^{-1}$.

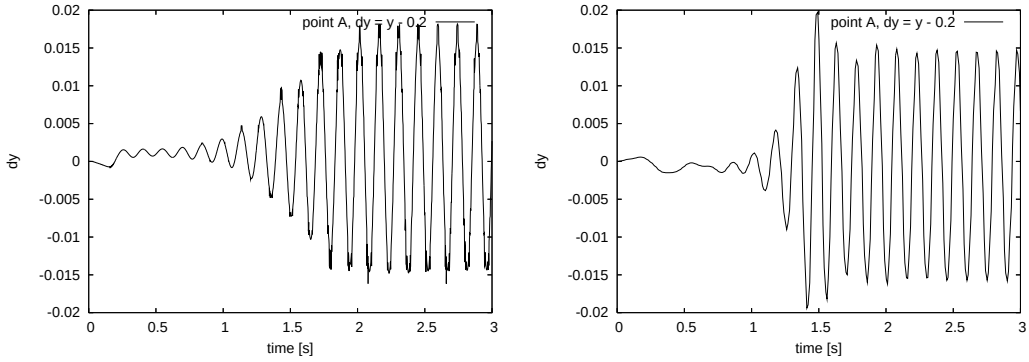

Figure 25: *FSI-3*: Vertical displacement of the control point A, obtained by the Eulerian approach (left) with max. amplitude $1.6 \cdot 10^{-2}$ and frequency $6.86\, s^{-1}$, and by the ALE approach (right) with max. amplitude $1.51 \cdot 10^{-2}$ and frequency $6.70\, s^{-1}$.*

9.4 FSI test with large deformations

In the test case FSI-2* (see Table 8) the fluid is initially in rest and the bar is subjected to a vertical (gravitational) force. This causes the bar to bend downward until it touches the bottom wall. A sequence of snapshots of the transition to steady

state obtained by the Eulerian approach for this problem is shown in Figure 26 for zonal mesh refinement. The position of the trailing tip A is show in Figure 27.

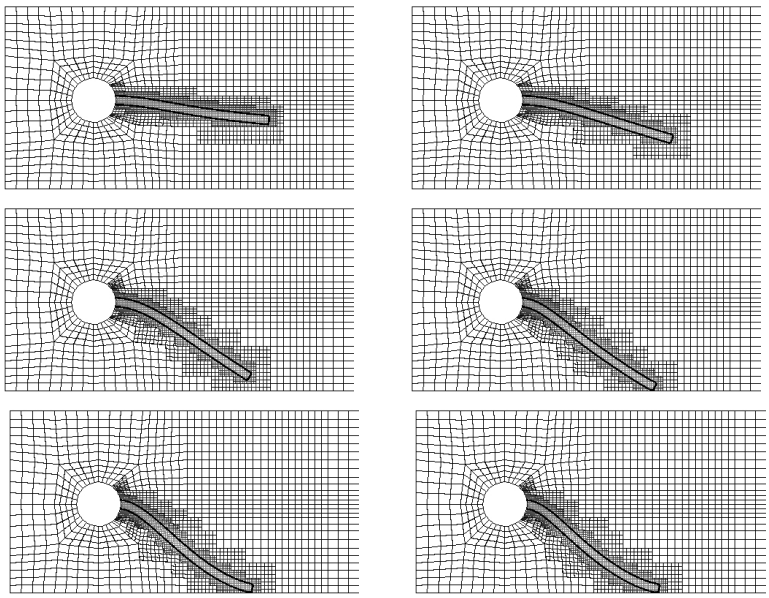

Figure 26: FSI-2*: A sequence of snap-shots of the bar's large deformation under gravitational loading obtained by the Eulerian approach.

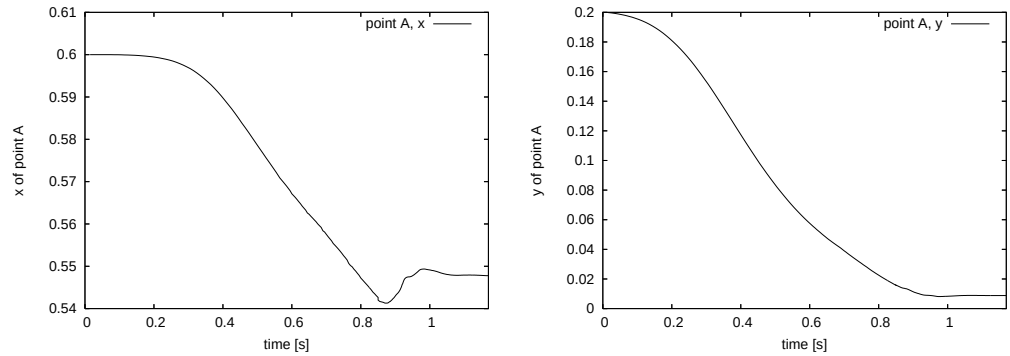

Figure 27: FSI-2*: Position of the control point A during the deformation of the bar: x-coordinate (left) and y-coordinate (right)

Finally, we compare the efficiency of zonal refinement versus local refinement by the DWR method for this test case. Figure 28 shows corresponding sequences of snapshots, while the position of the trailing tip A is displayed in Figure 29. We see that by sensitivity-driven local refinement within the DWR method on only 1 900 cells almost the same accuracy can be achieved as by zonal refinement on 12 300

cells. The gain in CPU time needed is almost 85 % (about 30 h for the zonal versus about 4 h for the local refinement).

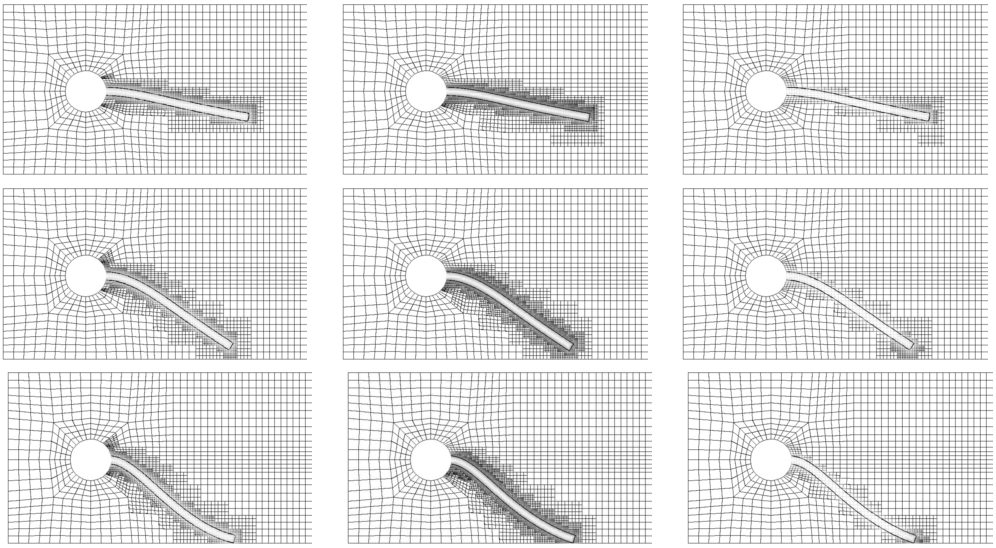

Figure 28: *A sequence of snap-shots of the bar's large deformation under gravitational loading obtained by the Eulerian approach using zonal refinement with* $N \sim 3\,000$ *and* $N \sim 12\,000$ *cells (left and midlde), and local mesh refinement by the DWR method (right) with only* $N \sim 1\,900$ *cells*

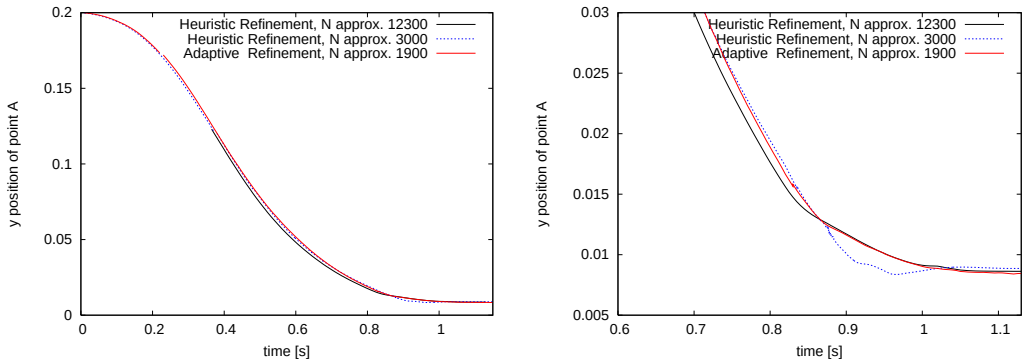

Figure 29: *Time varying position of the point* $x_A(t)$ *over the full time interval* $[0, 1.1]$ *(left) and over a zoomed interval* $[0.6, 1.1]$ *(right).*

10 Summary and future development

In this paper we presented a fully Eulerian (Eulerian) variational formulation for "fluid-structure interaction" (FSI) problems. This approach uses the "initial position" set (IP set) method for interface capturing, which is similar to the "level set" (LS) method, but preserves sharp corners of the structure. The harmonic continuation of the structure velocity avoids the need of reinitialization of the IP set. This

approach allows us to treat FSI problems with free bodies and large deformations. This is the main advantage of this method compared to interface tracking methods such as the arbitrary Lagrangian-Eulerian (ALE) method. At several examples the Eulerian approach turns out to yield results which are in good agreement with those obtained by the ALE approach. In order to have a "fair" comparison both methods have been implemented using the same numerical components and software library GASCOIGNE [26]. The method based on the Eulerian approach is inherently more expensive than the ALE method, by about a factor of two, but it allows to treat also large deformations and some kinds of topology changes.

As already mentioned above, theoretical results on existence of solution for fluid-structure interaction problems are rather sparse in the literature and can be found only for certain reduced systems and under very restrictive assumptions on the smallness of the data. The following list though is by far not comprehensive. Many results are available based on interaction of fluid with fixed rigid structures. In Desjardins and Esteban [18, 19] the authors show that solutions exist for a finite number of rigid non-colliding structures embedded in the fluid. The considered fluids are incompressible as well as compressible isentropic fluids modeled by the Navier-Stokes equations. Previous work in this direction can be found in Desjardins [17]. Using an approach similar to that in Desjardins and Esteban [18, 19] the authors of Desjardins, Esteban, Grandmont, and LeTallec [20] prove the existence of weak solutions for an instationary fluid-elastic structure interaction model. This is achieved by "Leray's method", i.e., by finding weak solutions that satisfy bounds for the energy of the complete system. The authors model the elastic structure as a compressible linearized neo-Hookean material with a finite number of elastic modes. In LeTallec and Mani [42] the authors investigate an instationary linearized fluid-structure interaction problem for a viscous fluid and a thin elastic shell with small displacements. The authors simplify the problem by neglecting changes to the geometry. Based on these premises by using energy estimates they show that the problem is well posed, that a weak solution exists and that the discrete approximation, based on their discretization, converges to the continuous solution.

The monolithic variational formulation of the FSI problem provides the basis for the application of the "dual weighted residual" (DWR) method for "goal-oriented" a posteriori error estimation and mesh adaptation. In this method inherent sensitivities of the FSI problem are utilized by solving linear "dual" problems, similar as in the Euler-Lagrange approach to solving optimal control problems. The feasibility of the DWR method for FSI problems has, in a first step, been demonstrated for the computation of steady state solutions.

One conceptional disadvantage of the Eulerian approach to treating FSI problems is the need for a time-independent outer domain Ω, in which the FSI process takes place. This seems to prevent the use of this approach for simulating flow through blood vessels since here the time-varying vessel wall forms the "outer domain". This difficulty can be cured by embedding the whole vessel into an outer softer medium, as seems realistic from the biological point of view. The physical properties of this outer medium have to be provided by biomedical experience. The realization of this concept is the subject of ongoing research. The following topics have to be worked on in the future:

- The DWR method has to be applied also for nonstationary FSI problems, particularly for the simultaneous adaptation of spatial mesh and time step size.
- Another goal is the development of the Eulerian approach for three-dimensional FSI problems and to explore its potential for FSI problems with large deformations and topology changes, such as occurring in heart-valve simulations
- Application to optimal control problems with FSI

$$\min_{q \in Q} J(u,q)\,! \qquad a(u,q)(\psi) = f(\psi) \quad \forall \psi \in \mathcal{V}^0.$$

  In the context of the "all-at-once" approach (KKT System) goal-oriented error estimation is "relatively cheap".

11 Acknowledgement

This work has been supported by the Deutsche Forschungsgemeinschaft (DFG), Research Unit 493 "Fluid-Struktur Interaction: Modeling, Simulation, Optimization". This support is gratefully acknowledged.

References

[1] G. Allaire, F. de Gournay, F. Jouve, and A. Tonder, *Structural optimization using topological and shape sensitivities via a level set method*, Control and Cyb. 34, 59–80 (2004).

[2] W. Bangerth and R. Rannacher, *Adaptive Finite Element Methods for Differential Equations*, Birkhäuser, 2003.

[3] R. Becker and M. Braack, *Multigrid techniques for finite elements on locally refined meshes*. Numer. Linear Algebra Appl. 7, 363–379 (2000).

[4] R. Becker and M. Braack, *A finite element pressure gradient stabilization for the Stokes equations based on local projections*, Calcolo 38, 173-199 (2001).

[5] R. Becker and M. Braack, A two-level stabilization scheme for the Navier-Stokes equations, *Proc. ENUMATH-03*, pp. 123-130, Springer, 2003.

[6] R. Becker, V. Heuveline, and R. Rannacher, *An optimal control approach to adaptivity in computational fluid mechanics.* Int. J. Numer. Meth. Fluids. 40, 105–120 (2002).

[7] R. Becker and R. Rannacher, Weighted a-posteriori error estimates in FE methods, Lecture ENUMATH-95, Paris, Sept. 18-22, 1995, in: *Proc. ENUMATH-97*, (H.G. Bock, et al., eds), pp. 621-637, World Scientific Publ., Singapore, 1998.

[8] R. Becker and R. Rannacher, An optimal control approach to error estimation and mesh adaption in finite element methods, *Acta Numerica 2000* (A. Iserles, ed.), pp. 1-101, Cambridge University Press, 2001.

[9] R. Becker and R. Rannacher, *A feed-back approach to error control in finite element methods: basic analysis and examples*, East-West J. Numer. Math. 4, 237-264 (1996).

[10] M. Braack and Th. Richter, *Solutions of 3d Navier-Stokes benchmark problems with adaptive finite elements*, Computers and Fluids 35, 372–392 (2006).

[11] D. Braess, *Finite Elements*, Cambridge University Press, Cambridge, United Kingdom, 1997.

[12] S. Brenner and R. L. Scott, *The Mathematical Theory of Finite Element Methods*, Springer, Berlin Heidelberg New York, 1994.

[13] M. O. Bristeau, R. Glowinski, and J. Periaux, Numerical methods for the Navier-Stokes equations, *Comput. Phys. Rep.* 6, 73-187 (1987).

[14] H.-J. Bungartz and M. Schäfer (eds), *Fluid-Structure Interaction: Modeling, Simulation, Optimization*, Springer, Berlin-Heidelberg, 2006.

[15] G. Carey and J. Oden, *Finite Elements, Computational Aspects*, volume III. Prentice-Hall, 1984.

[16] Y. C. Chang, T. Y. Hou, B. Merriman, and S. Osher, A level set formulation of Eulerian interface capturing methods for incompressible fluid flows, *J. Comp. Phys.* 123, 449-464 (1996).

[17] B. Desjardins, *On weak solutions of the compressible isentropic Navier-Stokes equations*, Applied Math. Letters 12, 107–111 (1999).

[18] B. Desjardins and M. J. Esteban, *Existence of weak solutions for the motion of rigid bodies in a viscous fluid*, Arch. Rat. Mech. Anal. 146, 59–71 (1999).

[19] B. Desjardins and M. J. Esteban, *On weak solutions for fluid-rigid structure interaction: compressible and incompressible models*, Comm. P.D.E. 25, 1399–1413 (2000).

[20] B. Desjardins, M. J. Esteban, C. Grandmont, and P.Le Tallec, *Weak solutions for a fluid-elastic structure interaction model*, Rev. Mat. Comput. 14, 523–538 (2001).

[21] Th. Dunne, *An Eulerian approach to fluid-structure interaction and goal-oriented mesh refinement*, Proc. "Finite Elements for Flow Problems (FEF05)", IACM Special Interest Conference supported by ECCOMAS, April 4-6, 2005, Swansea, Wales, UK, Int. J. Numer. Methods Fluids 51, 1017–1039 (2006).

[22] Th. Dunne, *Adaptive Finite Element Simulation of Fluid Structure Interaction Based on an Eulerian Formulation*, Doctoral dissertation, Institute of Applied Mathematics, University of Heidelberg, 2007.

[23] Th. Dunne, *Adaptive Finite Element Simulation of Fluid Structure Interaction Based on an Eulerian Formulation*, Vieweg+Teubner Series Advances in Numerical Mathematics, to appear 2009.

[24] Th. Dunne and R. Rannacher, *Adaptive finite element simulation of fluid-structure interaction based on an Eulerian variational formulation*, in "Fluid-Structure Interaction: Modeling, Simulation, Optimization" (H.-J. Bungartz and M. Schäfer, eds), pp. 371–386, Springer, Berlin-Heidelberg, 2006.

[25] K. Eriksson, D. Estep, P. Hansbo, and C. Johnson, Introduction to adaptive methods for differential equations. *Acta Numerica 1995* (A. Iserles, ed.), pp. 105–158, Cambridge University Press, 1995.

[26] GASCOIGNE, A C++ numerics library for scientific computing, Institute of Applied Mathematics, University of Heidelberg, URL `http://www.gascoigne.uni-hd.de/` .

[27] V. Girault and P.-A. Raviart, *Finite Element Methods for the Navier-Stokes Equations*, Springer: Berlin-Heidelberg-New York, 1986.

[28] R. Glowinski, Finite element methods for incompressible viscous flow, in *In Handbook of Numerical Analysis Volume IX: Numerical Methods for Fluids (Part 3)* (P.G. Ciarlet and J.L. Lions, eds), North-Holland, Amsterdam, 2003.

[29] A. Griewank, *On automatic differentiation in mathematical programming: recent developments and applications*, (M. Iri and K. Tanabe, eds), pp. 83–108, Kluwer Academic Publishers, 1989.

[30] M. Heil, A. L. Hazel, and J. Boyle, *Solvers for large-displacement fluid-structure interaction problems: segregated versus monolithic approaches.* Comput. Mech. 43, 91–101 (2008).

[31] J. Heywood, R. Rannacher, and S. Turek, *Artificial boundaries and flux and pressure conditions for the incompressible Navier-Stokes equations*, Int. J. Numer. Math. Fluids 22, 325–352 (1992).

[32] C. W. Hirt and B. D. Nichols, Volume of Fluid (VOF) method for the dynamics of free boundaries. *Journal of Computational Physics* 39, 201-225 (1981).

[33] J. Hron and S. Turek, *Proposal for numerical benchmarking of fluid-structure interaction between an elastic object and laminar incompressible flow*, in "Fluid-Structure Interaction: Modelling, Simulation, Optimisation" (H.-J. Bungartz and M. Schäfer, eds), Springer, Berlin-Heidelberg, 2006.

[34] J. Hron and S. Turek, *A monolithic FEM/multigrid solver for an ALE formulation of fluid-structure interaction with applications in biomechanics*, in "Fluid-Structure Interaction: Modelling, Simulation, Optimisation" (H.-J. Bungartz and M. Schäfer, eds), pp. 146–170, Springer, Berlin-Heidelberg, 2006.

[35] A. Huerta and W. K. Liu, *Viscous flow with large free-surface motion*, Computer Methods in Applied Mechanics and Engineering, 1988.

[36] T. J. R. Hughes and A. N. Brooks, *Streamline upwind/Petrov–Galerkin formulations for convection dominated flows with particular emphasis on the incompressible Navier-Stokes equation.* Comput. Meth. Appl. Mech. Engrg. 32, 199–259 (1982).

[37] T. J. R. Hughes, L. P. Franc, and M. Balestra, *A new finite element formulation for computational fluid mechanics: V. Circumventing the Babuska-Brezzi condition: A stable Petrov-Galerkin formulation of the Stokes problem accommodating equal order interpolation.* Comput. Meth. Appl. Mech. Engrg. 59, 85–99 (1986).

[38] T. J. R. Hughes, W. K. Liu, and T. K. Zimmermann, *Lagrangian-Eulerian finite element formulations for incompressible viscous flows*, Comput. Meth. Appl. Mech. Engrg. 29, 329–349 (1981).

[39] S. Geller, J. Toelke, and M. Krafczyk, *Lattice-Boltzmann methods on quadtree-type grids for fluid-structure interaction*, in "Fluid-Structure Interaction: Modelling, Simulation, Optimization" (H.-J. Bungartz and M. Schäfer, eds), pp. 270–293, Springer, Berlin-Heidelberg, 2006.

[40] D. D. Joseph and Y. Y. Renardy, *Fundamentals of two-fluid dynamics. Part I and II*, Springer, New York, 1993. Math. Theory and Applications.

[41] A. Legay, J. Chessa, and T. Belytschko, An Eulerian-Lagrangian method for fluid-structure interaction based on level sets, *Comp. Meth. in Applied Mech. and Engrg.*, 2004.

[42] P. Le Tallec and S. Mani, *Numerical analysis of a linarized fluid-structure interaction problem*, Numer. Math. 87, 317–354 (2000).

[43] C. Liu and N. J. Walkington, An Eulerian description of fluids containing viscoelastic particles, *Arch. Rat. Mech. Anal.* 159, 229–252 (2001).

[44] S. Osher and J. A. Sethian, Propagation of fronts with curvature based speed: algorithms based on Hamilton-Jacobi formulations, *Journal of Computational Physics* 79, 12 (1988).

[45] L. B. Rall, *Automatic Differentiation - Techniques and Application*, Springer, New York, 1981.

[46] R. Rannacher, Finite element methods for the incompressible Navier-Stokes equations, in *Fundamental Directions in Mathematical Fluid Mechanics* (G. P. Galdi, J. Heywood, R. Rannacher, eds), pp. 191–293, Birkhäuser, Basel-Boston-Berlin, 2000.

[47] R. Rannacher, Incompressible Viscous Flow, in *Encyclopedia of Computational Mechanics* (E. Stein, et al., eds), John Wiley, Chichester, 2004.

[48] R. Rannacher and F.-T. Suttmeier Error estimation and adaptive mesh design for FE models in elasto-plasticity, in *Error-Controlled Adaptive FEMs in Solid Mechanics* (E. Stein, ed.), pp. 5–52, John Wiley, Chichster, 2002.

[49] J.A. Sethian, *Level Set Methods and Fast Marching Methods.* Cambridge University Press, 1999.

[50] J. Sokolowski and J. P. Zolesio, *Introduction to Shape Optimization: Shape Sensitivity Analysis*, Springer, Berlin, 1992.

[51] T. E. Tezduyar, M. Behr, and J. Liou, A new strategy for finite element flow computations involving moving boundaries and interfaces-the deforming-spatial-domain/space-time procedures: I. The concept and preliminary tests, *Computer Methods in Applied Mechanics and Engineering*, 1992.

[52] T. E. Tezduyar, M. Behr, and J. Liou, A new strategy for finite element flow computations involving moving boundaries and interfaces-the deforming-spatial-domain/space-time procedures: II. Computation of free-surface flows, two-liquid ows and ows with drifting cylinders, *Computer Methods in Applied Mechanics and Engineering*, 1992.

[53] T. E. Tezduyar, S. Sathe, K. Stein, and L. Aureli, *Modeling of fluid-structure interaction with the space-time technique*, in "Fluid-Structure Interaction: Modelling, Simulation, Optimization" (H.-J. Bungartz and M. Schäfer, eds), pp. 50–81, Springer, Berlin-Heidelberg, 2006.

[54] S. Turek, *Efficient solvers for incompressible flow problems: an algorithmic and computational approach*, Springer, Heidelberg-Berlin-New York, 1999.

[55] S. Turek and M. Schäfer, Benchmark computations of laminar flow around a cylinder. In E.H. Hirschel, editor, 'Flow Simulation with High-Performance Computers II', volume 52 of *Notes on Numerical Fluid Mechanics.* Vieweg, 1996.

[56] J. Vierendeels, *Implicit coupling of partial fluid-structure interaction solvers using reduced-order models*, in "Fluid-Structure Interaction: Modelling, Simulation, Optimization" (H.-J. Bungartz and M. Schäfer, eds), pp. 1–18, Springer, Berlin-Heidelberg, 2006.

[57] VISUSIMPLE, An open source interactive visualization utility for scientific computing, Institute of Applied Mathematics, University of Heidelberg, URL `http://visusimple.uni-hd.de/` .

[58] W. A. Wall, *Fluid-Structure Interaction with Stabilized Finite Elements*, doctoral dissertation, Report No. 31 (1999), Institute of Structural Mechanics, University of Stuttgart.

[59] W. A. Wall, A. Gerstenberger, P. Gamnitzer, C. Forster, and E. Ramm, *Large deformation fluid-structure interaction: advances in ALE methods and new fixed grid approaches*, in "Fluid-Structure Interaction: Modelling, Simulation, Optimization" (H.-J. Bungartz and M. Schäfer, eds), pp. 195–232, Springer, Berlin-Heidelberg, 2006.